Implementing plant hydraulics in the Community Land Model

Daniel Kennedy[1], **Sean Swenson**[2], **Keith Oleson**[2], **David Lawrence**[2], **Rosie Fisher**[2], **Pierre Gentine**[1]

[1]Columbia
[2]National Center for Atmospheric Research, Table Mesa Drive, Boulder, Colorado, USA

Key Points:

- A simplified soil-plant-atmosphere continuum model based on hydraulic theory is implemented in the Community Land Model (version 5).
- Prognostic leaf water potential replaces soil matric potential as the functional basis for water stress, thus reflecting how the leaf water supply (via the xylem network) and evaporative demand act in concert to determine plant water status and thus stomatal conductance and leaf gas exchange.
- Prognostic root water potential is used to implement hydraulic root water uptake, replacing the heuristic soil 'wilting' factor .

Corresponding author: Daniel Kennedy, djk2120@columbia.edu

Abstract

= enter abstract here =

1 Introduction

Trees face emerging climate change risk globally [*Allen et al.*, 2010; *Anderegg et al.*, 2013a]. Understanding vegetation response is a high priority, both for discerning climate impacts and for modeling feedbacks to the carbon and hydrological cycles. In addition to stress from soil moisture drought, vegetation is susceptible to increasing atmospheric transpiration demand [*Restaino et al.*, 2016; *Novick et al.*, 2016a]. Increases in vapor pressure deficit (VPD) have occurred with warming [*Ficklin and Novick*, 2017; *Seager et al.*, 2015], and are associated with impacts on vegetation [*Williams et al.*, 2013; *Mcdowell and Allen*, 2015]. Significant uncertainty remains regarding how vegetation will respond to changes in hydroclimate within Earth System Models, feeding back onto the carbon cycle as vegetation mediates carbon uptake [*De Kauwe et al.*, 2017; *Friedlingstein et al.*, 2014].

Plant water stress parameterizations are important in Earth System Models, as they define vegetation regulation of surface fluxes (photosynthesis, transpiration) to water fluctuations. Vegetation water use strategies also modulate carbon uptake, creating a critical coupling between the Earth System's carbon and hydrological cycles [*Green et al.*, 2017]. Drought stress parameterizations (functions which relate simple metric of soil moisture status to leaf gas exchange) are widely used to define the response of stomatal conductance to vegetation water status that is used to attenuate transpiration, photosynthesis, and root water uptake with drying. The dynamics of water stress in models have broad effects on critical land surface processes [*Joetzjer et al.*, 2014]. On diurnal timescales, water stress parameterizations influence the partitioning of latent versus sensible heat with effects on surface temperature [*Bonan et al.*, 2014]. On longer timescales vegetation water use strategies regulate the global carbon and water cycles [*De Kauwe et al.*, 2015].

Many recent studies have aimed at advancing the representation of water flow through the Soil-Plant-Atmosphere continuum (SPAC) in land models [*Xu et al.*, 2016; *Christoffersen et al.*, 2016; *Sperry et al.*, 2017]. Explicit modeling of water flow through the SPAC adds complexity, but is consistent with evidence of dynamic regulation of vegetation water use in response to both soil and atmospheric drying [*Sperry and Love*, 2015]. Furthermore, via Darcy's Law, SPAC models have a robust physical basis. SPAC models involve new parameters, which presents new challenges [*Drake et al.*, 2017], but plant hydraulic trait information is available [*Kattge et al.*, 2011; *Anderegg*, 2015a], providing guidance on parameter estimation. and can be informative of forest vulnerability to drought [*Choat et al.*, 2012]. Likewise vegetation water status observations are available at a scale that is directly relevant to model development [*Konings et al.*, 2016; *Grant et al.*, 2016] and can be used to validate model results [*Momen et al.*, 2017; *Konings et al.*, 2017b].

The empirical representation of vegetation water stress in the Community Land Model (CLM) and other land surface models is a known deficiency, with implications for the representation of the dry/wet season in tropical rainforests [*Powell et al.*, 2013; *Ukkola et al.*, 2016].

In this study, we develop a plant hydraulic implementation within the recently released CLM version 5 (CLM5), based on hydraulic theory, which we refer to as the 'Plant Hydraulic Stress' (PHS) configuration. We analyse the dynamics of the new PHS model using site-level simulations that replicate the Caxiuanã, Brazil through-fall exclusion experiment [*Fisher et al.*, 2006].

Advancing the representation of the SPAC introduces the representation of vegetation water potential (discretized into leaf, stem and root elements) into the CLM, as well as an explicit representation of water supply, from the soil through the vegetation substrate. Tran-

spiration is attenuated with drought stress according to vegetation water status, capturing dynamic vegetation water use regulation. These changes have numerous implications, including

1. Leaf water potential serves as an improved metric for water status (compared to soil water or soil matric potential), since it reflects vegetation sensitivity to both soil and atmospheric drying, while serving as a diagnostic for excessive xylem tension and cavitation risk.

2. Modeling and plant hydrodynamics provides a framework for representing hydraulic redistribution [*Lee et al.*, 2005]

3. Modeling vegetation water potential allows improved connection to remote sensing observations (e.g. Vegetation Optical Depth) [*Konings et al.*, 2016].

4. Further, root water potential can be used to predict gradient-based root water uptake based on Darcy's law, replacing the previous empirical transpiration partitioning heuristic. This provides the means to vary, for example, the mean depth of extraction with changing soil water conditions.

5. The new model can represent a range of water use strategies, improving the connection between plant carbon allocation decisions and water availability.

SAY IN WHICH SECTION WE WILL FINE EACH PART

To assess the new model formulation, we carried out site-level simulations at Caxiuanã National Forest in Brazil, which features a critical biome (terra-firme moist tropical evergreen forest). Starting in 2001, a plot at this site was subjected to an approximately 50% percent precipitation through-fall exclusion. Due to the large drop in soil moisture at the precipitation exclusion site, we expect and observe [*Fisher et al.*, 2007] significant vegetation regulation of transpiration and photosynthesis.

In this paper we 1. Introduce the PHS theory and implemention in the CLM 2. Analyze the dynamics of modeled water stress, root water uptake and soil moisture profiles. 3. Compare PHS to the behaviour of the default CLM water stress configuration. 4. Discuss the benefits and limitations of the new model.

2 Model Description

2.1 Photosynthesis

The CLM5 photosynthesis model is described in *Bonan et al.* [2011], *Thornton and Zimmermann* [2007], and *Oleson et al.* [2013].Photosynthesis is defined in three regimes: Rubisco-limited, light-limited, and export-limited following *Farquhar et al.* [1980] and *Harley et al.* [1992].The implementation extends *Sellers et al.* [1996a,b] with co-limitation following *Collatz et al.* [1991].

CLM5 photosynthesis, in its default configuration, is a two-big-leaf model, with a sunlit and shaded leaf for each plant functional type [*Thornton and Zimmermann*, 2007; *Dai et al.*, 2004; *Oleson et al.*, 2013]. The canopy fluxes module iterates the solution for leaf temperature to satisfy the leaf surface energy balance, while environmental conditions are evolving. Within this, the photosynthesis module further iterates to solve for inter-cellular CO_2 concentration, balancing stomatal flux of CO_2 with photosynthetic assimilation flux of CO_2.

2.2 Stomatal Conductance

CLM5 implements the Medlyn stomatal conductance model, which reconciles the empirical and optimal approaches to modeling stomatal conductance [*Medlyn et al.*, 2011]. Stomatal conductance of CO_2 is thus directly related to net photosynthesis (A_n), CO_2 concentration at the leaf surface (C_a), and the square root of the vapor pressure deficit near the

leaf surface ($\sqrt{D}$).

$$g_s = g_0 + \left(1 + \frac{g_1}{\sqrt{D}}\right)\frac{A}{C_a} \tag{1}$$

The model features two parameters g_0 (μmol / m2 / s) and g_1 (kPa$^{0.5}$). The g_0 parameter is minimum stomatal conductance, representing cuticular and epidermal losses (small). The g_1 parameter relates to the marginal water cost guiding the optimization of carbon assimilation. These parameters are plant functional type dependent.

The Medlyn model, derived from stomatal optimization theory, predicts stomatal conductance to maximize assimilation relative to water costs ($A - \lambda E$), but does not resolve concurrent limitations to stomatal conductance associated with drought conditions. These water stress factors (in our case, f_w), are used to represent stomatal and non-stomatal limitation not captured by the leaf-level stomatal conductance model (which can be thought of as a prediction of maximum stomatal conductance in these cases). To represent soil drought, and its impact on diffusive fluxes, land surface models typically include a 'water stress factor'(f_w, dimensionless, 0 to 1, formerly β_t). Uncertainty remains within the literature for how to apply water stress factors to photosynthesis and/or stomatal conductance. [*Zhou et al.*, 2013; *Novick et al.*, 2016b; *Sperry and Love*, 2015].

In CLM, f_w multiplies the rate of maximum carboxylation (V_{cmax}) as described in *Oleson et al.* [2013]. Other models opt for soil-moisture based stomatal limitation (linking the stomatal conductance model slope parameter to soil moisture), however, *Lin et al.* [2018] found that only g_0 was sensitive to soil moisture (and not g_1). *Zhou et al.* [2013] suggest that changes in assimilation tend to exceed those predicted by modulating g_1 with soil moisture, but could be captured by changing V_{cmax}. Other field studies, however, suggest that V_{cmax} does not change with drought, whereby modeled V_{cmax} instead may implicitly account for mesophyll conductance changes [*Flexas et al.*, 2004].

In PHS, we opt for a simplified form of this stress approach, which seems to be consistent with field observations [*Lin et al.*, 2018]. Prognostic water stress (f_w, ranging from 0-1) attenuates stomatal conductance indirectly via multiplication of V_{cmax}. Water stress then lowers assimilation, which is coupled to stomatal conductance ([*Medlyn et al.*, 2011]).

f_w is modeled here as a function of leaf water potential (ψ_{leaf}) (see Section 2.3.3), with stress increasing as ψ_{leaf} becomes more negative. This reflects the concept of hydraulic safety, with vegetation avoiding excessive xylem tension associated with risk of cavitation.

Utilizing leaf water potential adopts a framework where stomatal conductance optimized for carbon gain is concurrently limited by hydraulic constraints [*Novick et al.*, 2016b]. As a result, low soil water (bottom-up stress) can induce leaf moisture stress due to limited water supply while high atmospheric VPD can also induce leaf moisture stress by propagating a drying into the xylem (top-down stress).

Much recent work has focused on alternative constraints on plant hydrodynamics, especially in response to drying soils [*Manzoni et al.*, 2013a; *Novick et al.*, 2016b; *Zhou et al.*, 2014]. This includes how plants manage the risk of cavitation associated with increasing xylem tension [*Sperry et al.*, 1998]. [*Sperry et al.*, 2017], for example, argue that theory based on hydraulic costs (define) could be used instead of optimizing of $A - \lambda E$. Otherwise, the marginal water cost might be adjusted based on soil water status by adjusting λ or Medlyn g_1 [*Manzoni et al.*, 2013a], but this may underestimate drought effects on photosynthesis *expand on this-RF*[*Zhou et al.*, 2013; *Lin et al.*, 2018]. A hybrid approach, combines stomatal optimization with hydraulic constraints and/or so-called non-stomatal limitation, where stress attenuates V_{cmax} or mesophyll conductance (both of which feed back through photosynthesis to lower stomatal conductance) [*Egea et al.*, 2011; *Novick et al.*, 2016b]. [*link this back to which options are used in PHS -RF*]

2.3 Plant Hydraulic Stress (PHS)

The PHS model within CLM5 uses hydraulic (Darcy's) law and a corresponding electrical circuit analogy (Figure 1), to model the flow of water through the SPAC. The hydraulic framework is used to diagnose water stress associated with increasing xylem tension and to calculate the root water uptake in each of (in this case) 20 vertically discretized soil layers.

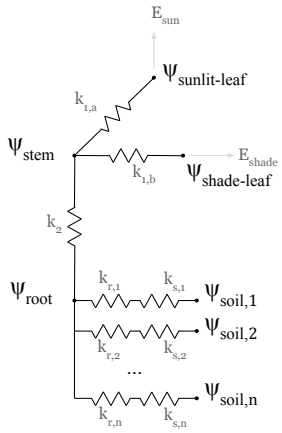

Figure 1. Plant hydraulic circuit analog schematic

2.3.1 Hydraulic schematic and segmentation

PHS solves for the set of SPAC vegetation water potential values (ψ_{root}, ψ_{stem}, $\psi_{\text{shade-leaf}}$, $\psi_{\text{sun-leaf}}$) that matches water supply (root water uptake) to water demand (transpiration), while maintaining continuity of water flow throughout the SPAC. Segmentation and other model design decisions followed a preference for a simplified implementation that whenever possible conformed to existing CLM model structure.

At each node in the circuit diagram in Figure 1 we model water potential, and, between nodes, we resolve the flux of water. The choice of nodes for segmentation is designed to take advantage of field-measured hydraulic traits and to allow for differences in segment parameterizations [*Simonin et al.*, 2015; *Sperry and Love*, 2015]. As in other versions of the CLM, PHS uses vertically discretized soil layers and a two-layer (sunlit vs. shaded) canopy. Water uptake from the different soil layers is assumed to operate in parallel; a typical assumption justified by higher resistance in lateral versus central roots (e.g. Williams et al. 2001). We further separate resistance through the soil matrix from the resistance through the root tissue [*Williams et al.*, 1996]. Specifics on the parameterization of conductance for each segment are provided in Appendix B.1.

2.3.2 Water supply

Water supply is modeled via Darcy's Law, where flow of water (q) is the product of the path hydraulic conductance (k) and the gradient in water potential (accounting for changes in gravitational potential). Equation 2 represents the flow from a generic node 1 to node 2.

$$q = -k\left(\psi_2 - \psi_1 - \rho g \Delta z\right) \tag{2}$$

PHS does not represent plant tissue water storage (or capacitance, using the electrical circuit analogy). Capacitance significantly complicates the water potential solution [*Celia et al.*, 1990] and is challenging to parameterize [*Bartlett et al.*, 2016]. However, buffering

of water stress provided by tissue water storage could potentially be important especially on sub-daily timescales [*Meinzer et al.*, 2009; *Epila et al.*, 2017], whereby its inclusion may be warranted in future model generations.

Vegetation segment conductance is modeled following empirical xylem vulnerability curves [*Tyree and Sperry*, 1989], where segments lose conductance with increasing xylem tension related to cavitation and embolism [*Holbrook et al.*, 2001]. The vulnerability curves model loss of conductance relative to maximum conductance using two parameters: c_k, a sigmoidal shape-fitting parameter, and p_{50}, the water potential at 50% loss of segment conductance (following *Gentine et al.* [2016]).

Both c_k and p_{50} can be estimated from field experiments [*Sack et al.*, 2002], and p_{50} is available in the TRY trait database [*Kattge et al.*, 2011]. Parameterization based on p_{50} aligns with the call for a transition to models that use a wider range of plant functional trait data in their parameterization [*Anderegg*, 2015a]. The loss of xylem conductivity is based on lower terminal water potential (ψ_1) as is typical in other simplified models [*Xu et al.*, 2016], but may underestimate the integrated loss of conductivity [*Sperry and Love*, 2015].

$$k = k_{\max} 2^{-\left(\frac{\psi_1}{p_{50}}\right)^{c_k}} \tag{3}$$

PHS models root, stem, and leaf tissue conductances according to equation 3. The parameterization of $k_{\max}$ varies by hydraulic segment (see details in Appendix B1). The conductance across the soil matrix to the root surface follows *Williams et al.* [2001] and *Bonan et al.* [2014] and estimates a characteristic distance between the bulk soil and the root surface, to facilitate length-scaling of soil conductivity. Bulk soil resistivity is based on *Clapp and Hornberger* [1978] as described in *Oleson et al.* [2013]. Further details are provided in Appendix B1.

2.3.3 Water demand

Vegetation water demand and stomatal regulation is based on the Medlyn stomatal conductance model (see Section 2.2), which we adjust using the water stress factor f_w. As discussed earlier, f_w is based on leaf water potential [*Klein and Niu*, 2014], and multiplies V_{cmax}, thus attenuating photosynthesis, and thus also stomatal conductance and transpiration.

As leaf water potential declines (because of transpiration) and xylem tension increases, transpiration is attenuated relative to its maximal value. The maximum transpiration ($E_{\text{sun,max}}$, $E_{\text{shade,max}}$) is defined as the value that results from Medlyn stomatal conductance in the absence of water stress (achieved by setting $f_w = 1$). The fraction of maximum transpiration is modeled with a two-parameter sigmoidal function (Equation 4).

$$\begin{aligned} E_{\text{sun}} &= E_{\text{sun,max}} 2^{-\left(\frac{\psi_{\text{sun-leaf}}}{\psi_{50}}\right)^{c_k}} \\ E_{\text{shade}} &= E_{\text{shade,max}} 2^{-\left(\frac{\psi_{\text{shade-leaf}}}{\psi_{50}}\right)^{c_k}} \end{aligned} \tag{4}$$

Where ψ_{50}, is the leaf water potential at 50% loss of transpiration and c_k is a sigmoidal shape-fitting parameter.

We define f_w as the ratio of attenuated to maximal stomatal conductance (Equation 5). Maximum stomatal conductance ($g_{\text{s,sun,max}}$, $g_{\text{s,shade,max}}$) is computed as the stomatal conductance in the absence of water stress, i.e. $f_w = 1$. The attenuated stomatal conductance ($g_{\text{s,sun}}$, $g_{\text{s,shade}}$) is then the stomatal conductance associated with the PHS module water flow solution, which matches vegetation water supply with vegetation water demand (Section 2.3.4).

$$f_{\text{w,sun}} = \frac{g_{\text{s,sun}}}{g_{\text{s,sun,max}}}$$
$$f_{\text{w,shade}} = \frac{g_{\text{s,shade}}}{g_{\text{s,shade,max}}} \tag{5}$$

Whereas the water supply parameters (see Section 2.3.2) relate to hydraulic traits often measured in the field, the hydraulic demand parameters ψ_{50} and c_k reflect the emergent property of hydraulic limitations to transpiration and must be empirically derived (WHAT ABOUT PLC CURVES?).

CLM also features two empirical stomatal control parameters, which are the soil matric potentials where stomata are either fully closed (θ_{wilt}) or fully open (θ_{crit}) (see Section 3). Recent modeling studies have proposed different forms of relationship between stomatal regulation with water stress [*Sperry et al.*, 2017; *Xu et al.*, 2016; *Christoffersen et al.*, 2016] and thus this representation remains the topic of active research .

2.3.4 PHS solution

PHS solves for the set of vegetation water potential values (ψ) that matches water supply (root water uptake) to water demand (transpiration), while satisfying continuity across the four water flow segments (soil-to-root, root-to-stem, stem-to-leaf, and leaves-to-transpiration). At each time step, PHS computes the flux divergence f (representing the mismatch of flow in and out of each segment for a given set of vegetation water potential values ψ_i, and iteratively updates ψ until convergence is reached in terms of divergence, $f \to 0$.

$$\psi = \begin{bmatrix} \psi_{\text{sun}} \\ \psi_{\text{shade}} \\ \psi_{\text{stem}} \\ \psi_{\text{root}} \end{bmatrix} \tag{6}$$

$$f(\psi) = \begin{bmatrix} E_{sun} - q_{sun} \\ E_{shade} - q_{shade} \\ q_{sun} + q_{shade} - q_{stem} \\ q_{stem} - \sum_{j=1}^{n} q_{root,j} \end{bmatrix} \tag{7}$$

$$A = \frac{df}{d\psi} \tag{8}$$

While $|f| > 0$

$$\Delta\psi = A^{-1} f(\psi_i)$$
$$\psi_{i+1} = \psi_i + \Delta\psi \tag{9}$$

The numerics are tractable because f has analytical derivatives and A (a 4x4 matrix with six null entries) is easy to invert when well-conditioned. Supply and demand converge, because transpiration demand decreases with more negative leaf water potentials and supply increases with more negative leaf water potentials. Within a set of PHS iterations (9), transpiration is assumed to be linear with f_w.

The PHS loop is nested within iterations for intercellular CO_2 concentration and leaf temperature. The non-linear relationship between f_w and transpiration is resolved through iteration for converging f_w alongside intercellular CO_2. Details on the numerical implementation are provided in Appendix Section B.1.

3 Water stress factor, SMS vs. PHS

PHS alters the transpiration beta function (β_t, colloquially BTRAN ,Equation 10), SAY WAHT IT IS which is the phenomenological soil water stress function in used in prior versions of CLM, as described in *Oleson et al.* [2013]. Because the name β_t is associated with this specific plant hydrodynamics representation, we opt to rename the variable to the water stress factor f_w. Throughout this paper we refer to the original CLM plant hydrodynamics framework as SMS (soil moisture stress), as compared to the newer implementation described here, PHS (plant hydraulic stress). We adopt this terminology (in lieu of CLM4.5 vs. CLM5), because SMS is still deployable with CLM5. In this section we present the SMS version of f_w and outline the differences as compared to PHS

With PHS, we interpret f_w as a drought safety mechanism, attenuating stomatal conductance to avoid excessive xylem tension associated with very negative leaf water potential. As such, f_w is parameterized as a function of prognostic leaf water potential. With SMS, f_w is calculated based on soil matric potential, as a root-fraction weighted average potential departure from an empirical soil layer wilting factor (Equation 10). Recent studies suggest that the SMS parameterization introduces model bias in turbulent fluxes [*Bonan et al.*, 2014] and contributes to unrealistic drought response of photosynthesis and stomatal conductance [*Powell et al.*, 2013].

In SMS, the variable f_w is unitless, ranging from 0 to 1, with 1 corresponding to no water stress, and 0 corresponding to fully water stressed. It is calculated based on a root-fraction weighted average of soil layer wilting factor (w_i), which is a bounded linear function of soil water potential (ψ_i) relative to PFT parameters defining the soil potential with stomates fully open (ψ_o) and fully closed (ψ_c), among the soil layers $i = 1, \ldots, n$. Note that root fraction (r_i) sums to 1, by definition.

$$f_w = \sum_{i=1}^{n} r_i w_i \tag{10}$$

$$w_i = 0 \leq \frac{\psi_i - \psi_c}{\psi_o - \psi_c} \leq 1 \tag{11}$$

3.1 Root water uptake in SMS vs. PHS

Such parameterizations (WHICH ONES?) have primarily been examined with application to stomatal conductance, but they are also used to define vegetation soil water extraction. Each timestep, the transpiration flux solution must be distributed among the vertically discretized soil layers. In the SMS framework, the transpiration sink is partitioned by layer according to the soil layer wilting factor and root fraction.

In both stress parameterizations, f_w multiplies V_{cmax} to attenuate photosynthesis and stomatal conductance with soil water stress. With SMS, it is also directly used for modeling vegetation water extraction from the soil column. The total transpiration (T) is partitioned among the soil layers based on the f_w wilting factor. Within each soil layer, the contribution to total transpiration (q_i) depends on the layer root fraction and wilting factor, normalized by f_w:

$$q_i = \frac{r_i w_i}{f_w} T \tag{12}$$

Contrary to the heuristic SMS parameterization, the PHS implementation adopts a physically-based hydraulic framework, where the root water uptake (q_i) is the product of the hydraulic conductance (k_i) and the gradient in water potential (-$\Delta\psi$) driving the flow, i.e. obeying Darcy's law. That gradient is the difference between the root water potential (ψ_{root})

and the layer soil water potential (ψ_i), minus changes in gravitational potential, following Darcy's law.

$$\begin{aligned} q_i &= -k_i \Delta\psi \\ \Delta\psi &= (\psi_{\text{root}} - \psi_i - \rho g \Delta z) \end{aligned} \tag{13}$$

For comparison between SMS and PHS, we recast (12) into the hydraulic framework: defining $T_{\max}$, such that: $T = f_w T_{\max}$ to replace T in (12), and replacing w_i in (12) with the formula from (11).

$$q_i = \frac{T_{\max}}{\psi_o - \psi_c} r_i \left(\psi_i - \psi_c\right) \tag{14}$$

This yields SMS analogs for the hydraulic conductance and gradient terms of Equation 13.

$$\begin{aligned} k_i &= r_i \frac{T_{max}}{\psi_o - \psi_c} \\ \Delta\psi &= \psi_c - \psi_i \\ \text{constrained by:} \qquad \Delta\psi &= \begin{cases} 0 & \text{if } \psi_i < \psi_c \\ \psi_c - \psi_o & \text{if } \psi_i > \psi_o \end{cases} \end{aligned} \tag{15}$$

We use this formulation to discuss some of the implications for root water uptake from the former SMS parameterization of water stress (Equation 15).

3.2 Constant pulling potential

With SMS, that gradient is defined for each soil layer as the difference between the soil water potential in that layer (ψ_i) and a constant parameter, the soil water potential when stomata are fully closed (ψ_c). This parameter serves as the vegetation "pulling" potential for calculating the soil transpiration sink.

Using a constant wilting point is inconsistent with extensive evidence from the field of dynamic vegetation water potential, and cohesion tension theory (CITATIONS NEEDED) driving the transpiration flow. Likewise the values for ψ_c are quite negative, (-2.5 MPa for broadleaf evergreen tropical, BET, forests). *Fisher et al.* [2006] measured midday stem potential consistently higher than -0.5 MPa during the wet season, and on average -1.69 and -1.53 MPa during the dry season in the control and exclusion plots, respectively.

3.3 Conductance dynamics

In SMS, in lieu of dynamic vegetation water potential, intra-day SMS soil sink dynamics derive from a highly variable conductance (CLARIFY). As inferred in Equation 15, SMS conductance is modeled as a function of T_{max}, and three constant parameters. T_{max} is highly dynamic, responding to the diurnal course in transpiration demand. This is inconsistent with general principles of porous media flow, where conductivity is a function of the hydraulic architecture and its wetted status. Likewise, this representation of conductance does not represent the characteristic phenomenon where vessels lose conductance with drying.

3.4 No dependence on belowground carbon allocation

As is typical in water stress parameterizations, the SMS conductance is scaled by layer using an area basis, here using the relative vertical root fraction is used. With PHS, an absolute measure of root biomass is used (see Appendix Equation B.7), so that the belowground water cycle interacts with carbon allocation to the roots. An absolute measure better conforms with the physics of porous media flow and better responds to varying carbon allocation

strategies. For example, with SMS, if root mass doubles in every soil layer, the root access to water remains unchanged.

3.5 Lacks penalties for extraction from depth

Both PHS and SMS account for the effect of decreasing root area with depth (PHS, root area; SMS, root fraction), but PHS implements two other penalties for extracting water from deep in the soil column that are missing from SMS. The first is minor, but water extracted from depth must overcome gravity, amounting to about 0.01 MPa per meter in depth. This is missing from SMS and included with PHS. Likewise, SMS ignores the fact that hydraulic conductance is generally taken to scale with the inverse of conducting length. Deeper roots feature longer root tissue conducting length, and root spacing within the soil is less dense, requiring longer conducting distances across the soil matrix.In PHS, both these processes result in diminished hydraulic conductance (UNCLEAR).

3.6 Constraints

With SMS, the gradient in water potential is constrained between 0 and the range of soil potential between parameters for stomata fully open and closed (Equation 15). The upper constraint caps the gradient in water potential when soil potential reaches the value for stomata fully open (ψ_o=-0.65 MPa for BET). Darcy's Law predicts that the gradient in water potential would continue to increase until saturation matric potential. The lower constraint caps the gradient in water potential at zero, disallowing negative gradients. However, reversed water fluxes, caused by positive gradients in water potential from root to soil, have been observed in the field [*Burgess et al.*, 1998]. Both constraints are eschewed with PHS.

4 Experiment Description

All four simulations in this paper use the same development version of CLM5 (development version r270, https://github.com/ESCOMP/ctsm/releases/tag/clm4_5_18_r270).

The four simulations are used to assess the impact of the plant hydrodynamics model (PHS vs. SMS) on a through-fall experiment (i.e., with either ambient or 60% through-fall excluded), with all other model components and forcing shared. Simulations are run offline (uncoupled from an active atmospheric model), spanning from 2001 through 2003, utilizing the satellite phenology (SP) mode of CLM5 in which vegetation state (LAI, canopy height) is prescribed and biogeochemistry is inactive. All simulations start from the same initial conditions, which are obtained from a 9-year spin-up that repeats the PHS/Ambient simulation three times. To avoid duplication, descriptions of site characteristics, forcing data, and observational sap flux, can be found in *Fisher et al.* [2007].

4.1 Parameter Values and Through-fall Exclusion

Selected parameter values concerning vegetation hydrodynamics are presented in Table 1. All other parameters use the default values associated with the r270 version of CLM5. Informed by *Fisher et al.* [2008], we tuned soil hydraulic parameters and through-fall exclusion rates to reasonably capture the observed soil water dynamics (*Fisher et al.* [2007] Figure 4), Supplementary Figure A.2. Likewise, we tuned k_{max} and g_1 parameters to improve the fit to sap flux observations in the ambient simulation. The object of this paper is to present the dynamical impact of PHS to clearly describe model functionality. Model skill and parameter sensitivity will be assessed in follow-up studies.

Table 1. Select parameter values

CLM name	Full Name	Symbol	Value
kmax(1)	Maximum Sun Branch Conductance	$k_{1a,\max}$	4e-7 s^{-1}
kmax(2)	Maximum Shade Branch Conductance	$k_{1b,\max}$	4e-7 s^{-1}
kmax(3)	Maximum Stem Conductivity	$k_{2,\max}$	4e-7 m/s
krmax	Maximum Root Conductivity	$k_{r,\max}$	6.3e-9 m/s
psi50	Water potential at 50% loss of conductivity	ψ_{50}	-2.45 MPa
ck	Vulnerability shape parameter	c_k	3.95
smpso	Soil potential with stomata fully open	ψ_o	-0.647 MPa
smpsc	Soil potential with stomata fully closed	ψ_c	-2.5 MPa
medlyn_intercept	Medlyn intercept	g_0	100 μmol / m2 / s
medlyn_slope	Medlyn slope	g_1	7 $kPa^{0.5}$
n	Soil porosity	n	0.42
hksat	Saturated soil hydraulic conductivity	$k_{\mathrm{s,max}}$	1.5e-5 m/s
sucsat	Saturated soil matric potential	ψ_{sat}	461 Pa
bsw	Brooks-Corey parameter	b	6

[a]Table note text here.

5 Analysis Details

5.1 Water potential

Annual and diurnal cycles of vegetation water potential are presented. For the diurnal cycle, we average by timestep over the 91 days of SON, 2003, reporting curves for root, stem, shade-leaf, and sun-leaf water potential. For the annual cycle, we plot monthly mean midday (local time 12:00 to 14:00) sun-leaf water potential.

5.2 Stress factor, annual cycle

Monthly means are reported for transpiration, gross photosynthesis, and f_w, the water stress factor (Fig 3). For the water stress factor, we opt to report the midday water stress averaging over local time 12:00 to 14:00. Monthly mean observational sap flow is also shown, courtesy of *Fisher et al.* [2007], which reports details on scaling observations to stand level. Months were dropped that featured fewer than 5 days of data.

5.3 Stress factor, diurnal cycle

In Figure 4, we plot the diurnal cycle of the stress factor averaged over the 2003 dry season (SON) (I am not a big fan of sentences in Figure we show, better to say what ahppens and then refer to figure). Drivers of the stress function are examined in Figure 5. To highlight the response of stress to VPD, we subsetted data according to downwelling solar radiation, which also influences stress. Data are selected with downwelling solar radiation between 400 and 425 W/m2, which corresponds to 775 half-hour timesteps. For the TFE simulations, (Figure 5c,d), we additionally exclude data from 2001, because TFE was not initiated until November 2001, leaving 515 timsteps. Data are subdivided into terciles based on soil water (within each plot), and colored accordingly. The terciles are defined for each simulation in Table 2.

5.4 Hydraulic conductance

In Figures 6 and **??**, we compare conductance values derived from the PHS and SMS implementations. With SMS, k is not explicitly modeled, so instead we infer k, by dividing

393 **Table 2.** Root-zone soil potential terciles for Figure 5

Simulation	T1	T2
PHS, Ambient	-0.0136 MPa	-0.0476 MPa
PHS, TFE	-0.0788 MPa	-0.2454 MPa
SMS, Ambient	-0.0056 MPa	-0.2296 MPa
SMS, TFE	-0.6474 MPa	-1.8467 MPa

407 root water uptake q_i, by $\Delta\psi$ as defined in Equation 15. We interpret the constraint that $\Delta\psi$
408 be greater than or equal to zero to mean that conductance is zero in non-conforming cases,
409 which we extend to $k = 0$ when $\Delta\psi < 1$ kPa. For our analyses, we consider only points
410 when transpiration is greater than 4 W/m2, which improves the tractability of inferring con-
411 ductance, given that SMS root water uptake is precluded absent transpiration (REPHRASE).

412 For Figure 6a,b, conductance is plotted from Soil Layer 3 (spans from 6 to 12 cm be-
413 low ground), for all points during 2003 when transpiration is greater than 4 W/m2 (n=7752).
414 For Figure **??**a,b, conductance is averaged daily, subject to the same restrictions. Average
415 intra-day standard deviation is reported for FMA, by which we calculate a daily standard de-
416 viation of complying points, and report the average over the 89 days.

417 ### 5.5 Root water uptake

418 Vertical profiles of the rate of root water uptake are presented in Figures 7a and 8a, av-
419 eraged over SON and FMA, respectively. This is plotted as average cumulative rate of root
420 water uptake, starting at depth (8.6 meters). Time series of total root water uptake are also
421 provided (Figs 7b,c, 8b,c). We plot total cumulative water extracted from near the surface
422 over time in Figures 7b and 8b, accompanied by that extracted from depths beyond 20 cen-
423 timeters in Figures 7c and 8d. We chose 20 centimeters as the break point based on the ver-
424 tical profiles of root water uptake, and with a preference for not splitting any of the discrete
425 soil layers. Soil Layers 1-4 span 0 to 0.2 meters, and Soil Layers 5-20 span 0.2 to 8.6 meters.
426 Time series of total cumulative ambient precipitation are shown for comparison (Figs 7b and
427 8b).

428 ### 5.6 Hydraulic redistribution

429 Hydraulic redistribution refers to flows of water between soil layers through vegeta-
430 tion substrate. To calculate total HR, we sum the negative root water uptake fluxes ((i.e.,
431 root to soil fluxes) across all soil layers. Total HR, partitioned by month and by daytime
432 versus nighttime is shown in Figure 9. Note that over the course of a day or season, HR
433 can occur without net negative root water uptake. For example, hydraulic lift may occur at
434 night, moving water from deep in the soil column up to near the surface, which is then more
435 readily available for transpiration during the following day. This can result in HR occurring
436 even when there is net positive root water uptake. This type of feature is evident in Figure 7,
437 where there is net positive root water uptake throughout the soil column over the 2003 dry
438 season, even when there is significant HR into the near-surface layers (Fig 9).

439 ### 5.7 Soil moisture

440 The vertical profile soil water potential under 60% TFE is plotted in Figure 10 (SMA,
441 DO NOT SAY THIS IS PLOTTED BUT DESCIRBE RESULTS AND MENTION FIG-
442 URE). The range in soil potential is much larger within the SMS paradigm, which made it
443 difficult to plot both panels with the same color scale. In order to preserve information in

the PHS plot, we opt for a scale of 0 to -1 MPa, as compared to 0 to -3 MPa for SMS. When comparing column average soil potential, we use separate definitions, which reflect each paradigm's representation of soil water availability. With SMS, we opt for a root-fraction weighted average, following from Equation 14. This is a poor measure for PHS, because it neglects gravitational contributions and the appropriate root area basis. Instead we opt for predawn (defined at 5AM) root water potential, which, given minimal transpiration at night, is in equilibrium with the soil column.

6 Results and Discussion

6.1 Modeling vegetation water potential

The models are compared for the 2003 dry season (Sept-Oct-Nov or SON) at Caxiuana for two experiments: the first with ambient rainfall (AMB), and the second with 60% of rainfall excluded, or 'through-fall exclusion' (TFE), Figure 2.

In the ambient simulation (Fig 2a), average midday water potentials are -1.96, -1.95, -1.94 MPa for sunlit leaf, shaded leaf, and stem, respectively. With through-fall exclusion (TFE), as expected the midday water potentials decrease to -2.77, -2.76, -2.75 MPa, respectively (Fig 2b).

Both panels show the characteristic drop in water potential around midday and the expected sequencing with the leaf water potentials more negative than the stem potential, which is more negative than the root potential. The sequencing is difficult to distinguish from the plot, where the stem, sunlit, and shaded leaf water potential curves nearly overlap for both experiments because there is only very small drop in potential between the stem and leaves.

The small difference between leaf and stem water potentials results from minimal resistance to water flow across these segments. (LINK THIS TO THE PREVIOUS STATEMENT) The current PHS parameterization of stem-to-leaf resistance is relatively simple compared to the literature [*Franks et al.*, 2007] and could be advanced in future versions.

TFE lowers average midday sunlit leaf water potential by 0.81 MPa compared to the ambient simulation, during SON-2003 (dry season). This change in leaf water potential can be partitioned into the change in soil water potential, the change in potential drop from soil-to-root, and the change in potential drop from root-to-leaf.

Beginning with the change in soil water potential, in the ambient simulation, average predawn (5AM) root water potential (an integrated measure of soil water potential) is -0.075 MPa. With TFE, it falls to -0.36 MPa, resulting in a decrease in predawn root water potential of 0.28 MPa relative to the ambient simulation. The difference between midday and predawn root water potential (which stands in for potential drop from soil-to-root) is lowered by 1.06 MPa in the simulate TFE plot (from -0.06 MPa, ambient, to -1.12 MPA, TFE).

The difference between sunlit leaf and stem water potential at midday acts in the opposite direction, changing from -1.83 MPa in the ambient simulation to -1.29 MPa with TFE, attenuating the drop in leaf water potential by 0.54 MPa.

Predicted water potential values are comparable with field observations, where average dry season leaf water potential was measured as -2.47 MPa [*Fisher et al.*, 2006]. With PHS, modeled change in leaf water potential due to TFE is -0.81MPa, which can be partitioned into -0.28 MPa predawn root water potential, -1.06 soil-to-root drop, +0.53 root-to-leaf drop. The drop in water potential across the stem partially abates the change in the soil and roots due to TFE.

Though stem conductance decreases with drying, transpiration also decreases, yielding a net effect of a smaller drop in water potential across the stem. This is consistent with findings in *Fisher et al.* [2006] that most of the whole-plant resistance is above ground, but

that added resistance from drying is predominately sourced? below ground. Likewise *Fisher et al.* [2006] found evidence of isohydric behavior, where plants manage water loss through stomata to regulate leaf water potential, which is consistent with results here of reduction in potential drop across the stem. However, PHS shows declines in midday leaf water potential due to TFE, but *Fisher et al.* [2006] found no significant observed difference between ambient and TFE dry season leaf water potential. This could indicate that our parameters do not result in sufficiently isohydric behavior.

Many facets of our hydraulic representation are simplified relative to the literature, reflecting that in a model designed to operate at the global scale, there is a tradeoff between added complexity and parameter reduction. The current PHS parameterization omits vegetation capacitance, which may be important for accurately modeling the diurnal cycle of water stress especially in tropical rainforests [*Meinzer et al.*, 2009]. Further, hydraulic conductance hysteresis and permanent cavitation are absent from the PHS vulnerability parameterization, whereby xylem segments fully regain conducting capacity upon re-wetting. This limits the influence of drought legacy, which has been shown to be significant for forest mortality [*Anderegg et al.*, 2013b].

Similar to other simplified models [*Xu et al.*, 2016], loss of conductance is based on lower terminus water potential, which may underestimate integrated loss of conductivity [*Sperry and Love*, 2015]. These simplifications each serve to lessen the parameter and/or computational burden of PHS. Our objective was to simplify the plant hydraulic representation for this initial implementation, acknowledging that more comprehensive process representation may prove necessary for future model versions.

6.2 Stress factor, annual dynamics

Figure 3 shows monthly mean values of the water stress factor, gross primary productivity, and transpiration over the three-year simulations for PHS versus SMS under ambient and 60% through-fall exclusion conditions. Under ambient through-fall conditions, the SMS simulation features less stress (Fig 3b), with no stress (f_w>0.99) in 24 out of 36 months.

PHS predicts more stress (Fig 3a), with stress in sync with the evolution of midday leaf water potential (Figure 2). As a result, f_w is generally lowest in September (Fig 3e). ZQZ need to go back and output btran proper. Alternatively, SMS predicts no stress (f_w>0.99) during any of the three Septembers of the ambient simulation. Instead f_w is generally lowest in December.

SMS has the most stress in December, which is associated with lower soil moisture (Supp Fig **??**). While soil moisture is lowest in December, transpiration demand is higher in September, which is the month with the most stress in the PHS simulations (Fig3a). To achieve high transpiration rates, vegetation must operate with a large gradient in water potential from soil-to-leaf, associated with increased xylem tension and risk of cavitation. As such, leaf water potential declines with soil moisture drying, but also with increasing transpiration demand (Fig 2). PHS is designed to represent hydraulic limitation to transpiration associated with xylem tension, which responds to both soil drying and increased transpiration demand (i.e. higher VPD) [*Sperry and Love*, 2015]. The latter is absent from the SMS formulation.

Through-fall exclusion (which initiates on November 1, 2001) adds stress in both the SMS and PHS simulations (Fig3c,d) . The added stress is greater and the onset faster with SMS. In both cases, the effect of TFE accumulates in time, with less photosynthesis and transpiration in 2003 compared to 2002. This is not reflected in the sap flux observations, which feature a more rapid onset of reduced transpiration, and similar transpiration between 2002 and 2003.

In both SMS and PHS, soil water is used to buffer shortfalls in precipitation versus transpiration (Supp Fig A.11). (UNLCEAR). Transpiration in PHS is less sensitive to TFE, which can be partly attributable to differences in root water uptake (see Section 6.5). PHS utilizes more deep soil water to mitigate declines in root-zone soil moisture as water flow is imposed to go down water potential gradients. In the dry season surface drying also decreases soil-root conductance so that it is easier to extract moisture from deeper layers, consistent with observations based on isotopes (CITATION).

Another dynamic feature of PHS is that hydraulic limitation establishes a negative feedback loop between photosynthesis/transpiration and water stress. If photosynthesis increases, generally stomatal conductance and transpiration increase. This causes more negative leaf water potential and an associated increase in water stress, which attenuates photosynthesis. This diminishes variability in transpiration and photosynthesis, relative to SMS (Fig 3c-f). The strength of this feedback is subject to parameters controlling maximum conductance and the stomatal response to leaf water potential. Quantifying variability in diffusive fluxes with PHS as compared to SMS and observations is an important topic for future studies (See Lawrence et al in prep).

Significant uncertainty exists in soil and root hydraulic parameters as well as the root distribution, whereby better behavior may exist within the plausible parameter space. Likewise, the parameter values for both stress implementations could be tuned further. Observations indicate the trees here adopt an isohydric behavior, where declines in soil moisture are tightly coupled with reduced transpiration, which mitigates decreases in leaf water potential [*Fisher et al.*, 2006]. The parameter values employed for these simulations may be insufficiently isohydric (GIVE REFERENCE AND DEFINE ISOHYDRICITY), which could explain limited sensitivity to TFE relative to observations.

6.3 Stress factor, diurnal dynamics

In addition to changes in the annual cycle, PHS introduces a diurnal cycle to f_w (Fig 4a). The SMS version of f_w exhibits almost no diurnal variability (Fig 4b) since water stress is therein a function of soil water potential, which lacks a significant diurnal cycle. PHS uses a function of leaf water potential (e.g. Fig 2a,b) to model water stress, which responds to diurnal variation in transpiration demand (via changes in VPD, solar radiation, etc.).

The relationship of water stress with VPD and soil potential is shown in Figure 5. To emphasize the relationship with VPD, data are subsetted for a small window in downwelling solar radiation (between 400 and 425 W/m2). For the TFE simulations (panels *c* and *d*), we also subset for years 2002 and 2003, because TFE was not active during most of 2001. Points are colored based on soil potential, partitioning the data from each plot into terciles, blue points are wettest, red points driest, and yellow points intermediate. For details on the soil water classification and radiation subsetting see Section zqz (THIS SHOULD BE IN CAPTION NOT MAIN TEXT).

The SMS version of f_w has a clear dependence on soil potential, but no relationship with VPD (Fig 5b,d), as expected. Drier soil potentials are associated with lower values of f_w (which corresponds to more stress). With PHS, higher VPD results in more stress (Fig5a,c). Under ambient through-fall conditions (Fig5a), soil water potential has minimal influence. With TFE, stress responds to both VPD and soil water (Figure 5c). Similar effects are shown in response to downwelling solar radiation (Supp Fig A.3).

Water stress is applied to capture limitations with declining water status that are not reflected within the Medlyn stomatal optimization theory (which only optimizes $\delta E/\delta A$, and thus does not take water supply into account). CLM implements non-stomatal limitation by multiplying V_{cmax} by f_w. Though there is limited evidence of down-regulation of V_{cmax} [*Flexas et al.*, 2006], this was the best option within CLM for applying stress through the GPP term of the stomatal conductance model, in accordance with field observations [*Lin*

et al., 2018; *Zhou et al.*, 2013]. If in future versions of CLM, mesophyll conductance is represented, it may be a more appropriate avenue for achieving the same effect. (MERGE WITH PREVIOUS DISCUSSION, TRY AVOIDING REPETITIONS A MUCH AS POSSIBLE)

Total soil water content (or departure from saturation) is a typical basis for diagnosing water status and stress [*Drake et al.*, 2017], which is in line with an SMS-type approach. While capturing supply limitations, this framework neglects effects of transpiration demand on xylem tension. Given constant stomatal conductance, xylem tension increases with declining soil water, but also with increasing vapor pressure deficit. While VPD sensitivity is included in the Medlyn model, it serves to mitigate increasing water costs, without consideration of cavitation. Evidence suggests that vegetation employ water use strategies to mitigate the risk of cavitation associated with increasing xylem tension [*Sperry et al.*, 1998; *Fisher et al.*, 2006; *Choat et al.*, 2012]. Utilizing leaf water potential as the basis for water status reflects this constraint. This may be especially important given projected increases in VPD associated with warming.

6.4 Hydraulic conductance: PHS vs SMS (implied)

Soil-to-root conductance (k_{sr}) is explicitly represented in PHS, modeled as a function of soil potential (zqz). With SMS, k_{sr} is not explicitly modeled, but it can be inferred, by dividing root water uptake by the gradient in water potential (see Section zqz). Comparing conductance under these two paradigms serves to highlight differences in how water supply is modeled. In , we plot the time-series of conductance values from Soil Layer 3 (spanning from 6 to 12 centimeters below the surface) under ambient through-fall conditions during 2003, along with precipitation over the same period (PLUG IN CAPTION).

During the wet season, PHS conductance is greater than SMS by more than two orders of magnitude (Fig 6a,b). PHS conductance is generally steady through the wet season (Fig 6a), followed by a slow decline over the dry season with short resurgence episodes associated with rain events. The SMS implied conductance features more variability relative to the mean (Fig 6b). During FMA-2003, average intra-day standard deviation of Layer 3 conductance is 4.6e-12 s^{-1} with PHS and 9.9e-12 s^{-1} with SMS. In an absolute sense the SMS standard deviation is about twice as large as PHS. The difference is larger in a relative sense, as this corresponds to 0.08% of the mean FMA conductance with PHS and 62.9% of the mean FMA conductance with SMS.

The SMS inferred conductance is tethered to transpiration (see Section 3), which leads to the high variance and a clear diurnal cycle (Supp Fig A.5). Instead PHS calculates k_{sr} based on soil hydraulic properties and root xylem vulnerability, which better reflects the physics (flow has to be down water potential gradients) and the temporal dynamics of transpiration demand.

As a result conductance is less variable, with the expected responses to drydown (loss of conductance) and re-wetting (increased conductance). This is further demonstrated in Figure 7, where we plot the daily mean conductance from Soil Layer 3. With 60% through-fall exclusion (Fig7a, dotted line), PHS conductance decreases, whereas with SMS, the daily mean conductance increases (Fig7b). The latter SMS increase is unrealistic and conflicts with extensive literature demonstrating loss of conductivity with drying (CITATIONS).

Despite two orders of magnitude difference in conductances, total root water uptake during FMA2003 is not very different (23.4 cm PHS vs. 24.9 cm SMS). The reason for these smaller differences, is that the extraction gradient compensate for the differences in conductance. The SMS extraction gradient is measured relative to ψ_c (a parameter defining soil potential with stomates fully closed), which equals -2.5MPa for BET. The PHS extraction gradient is relative to root water potential which during 2003 (ambient through-fall) varies between -0.02 and -0.23 MPa. *Fisher et al.* [2006] measured stem water potential consistently higher (less negative) than -0.5MPa.

With TFE, PHS Layer 3 conductance can approach the values seen in SMS. The average Layer 3 conductance with PHS for August 2003 (60%TFE) is 4.75e-11 s^{-1} as compared to 3.89e-11 s^{-1} for SMS. This is a result of the orders of magnitude response of PHS soil-to-root conductance to changes in soil potential (Supp Fig A.6) (UNCLEAR MODIFY SENTENCE). This conforms with typical soil hydraulics, where large changes in conductance occur with drying. On the other hand, SMS conductance has no clear relationship with soil potential (Supp Fig A.6).

6.5 Root Water Uptake: PHS vs SMS

Root water uptake is the flux of water (q_i, mm/s) extracted from each of the vertically discretized soil layers ($i = [1, 2, ..., n]$). These fluxes are used as the soil transpiration sink terms within the Richards' equation [*Oleson et al.*, 2013] and, summed over the soil column, are equivalent to the transpiration flux. As described above (and in Section 3), PHS adopts a hydraulic framework for root water uptake.

PHS simulations (black color), feature more surface extraction than with SMS, especially under ambient through-fall conditions (Fig7a), during the 2003 dry season. The time-series of PHS total cumulative extraction (cm) from near-surface soil (Fig7b) responds to precipitation (Fig7d), with increased surface extraction after rain events.

Under ambient conditions the SMS partitioning of extraction between near-surface and depth is not sensitive to precipitation. In PHS near-surface extraction decreases by 40% with TFE (8.12 vs 13.51 cm), while, SMS features a 24% increase in absolute terms (5.28 vs 6.55 cm, Fig 7b). Under TFE, both PHS and SMS extract minimal water from between 0.5 and 4m, (3.18 cm and 0.56 cm, respectively, over the three months). Both compensate by increasing extraction from below 4m, but PHS to a much larger extent, which corresponds to overall significantly more root water uptake during TFE.

Root water uptake dynamics respond to changes in hydraulic conductance and/or changes in the gradient in water potential. PHS has more access to water at depth under TFE, associated with higher conductance values. With decreasing soil potential, hydraulic conductance decreases with PHS, but can increase with SMS (6.4). Instead SMS is limited by the extraction gradient, with root water uptake declining to zero as soil potential approaches -2.5 MPa (Supp Fig A.7). PHS is more sensitive to changes in soil water potential, with stronger decreases in root water uptake in response to drying within a soil layer (Supp Fig A.7). In response, PHS features increases in near-surface water uptake after rain and decreases with TFE.

The wet season (Feb-Mar-Apr FMA-2003), features more and steadier rain (Fig 8d). PHS responds with an increase in the proportion of water extraction from near the surface relative to SON. Under ambient conditions net extraction is zero beyond about 38 centimeters depth (Fig 8a, solid black line). In comparison, SMS extracts more than half its water from beyond 1 meter in depth even during the wet season (Fig 8a, solid gray line). With TFE, PHS extraction is negative beyond 20 centimeters, indicating hydraulic redistribution (Fig 8c). Over the three month FMA-2003 period, there is no net root water uptake below 20 centimeters depth, but rather a deposition of about 10 cm of water is simulated.

In both the wet and dry season, PHS features significantly more root water uptake from the near-surface layers (0 to 20cm in depth). Modeled surface extraction is especially high over the wet season under through-fall exclusion conditions, summing to 32.7 cm over 89 days. By comparison SMS extracts 4.8 cm under the same conditions. With a soil porosity of 0.42, the top 20 cm of soil hold only 8.2cm of water at saturation.

Conductances are higher with PHS (see Section 6.4), which allows for higher rates of root water uptake, especially from moist soil layers. Likewise PHS better reflects penalties for extraction from depth (Section 3, favoring near-surface water all else being equal. The

highest rates of root water uptake (relative to layer size) occur from Soil Layer 2, after rain events during the dry season (Supp Fig A.7). Lowering maximum conductance can attenuate high rates of extraction, if observations conflict with model output.

The PHS configuration allows for more realistic root water uptake, incorporating hydraulic theory. SMS does not accurately represent xylem loss of conductance or the dynamics of vegetation water potential. Both are difficult to parameterize, given the scarcity of data describing states, traits, and fluxes underground. PHS offers a process connection between soil potential and leaf water potential, which may be used to evaluate the model.

6.6 Hydraulic redistribution

During the wet season surface extraction supplies transpiration, but is also redistributed into lower soil layers. Hydraulic redistribution has been observed in the field [*Oliveira et al.*, 2005], and is not represented in the SMS version of the CLM [*Lee et al.*, 2005]. which sets root water uptake to zero if the gradient in water potential is negative.

For HR to occur into a soil layer, the soil potential must be more negative (drier) than the ψ_{root} (see Figure . During the day, transpiration requires a gradient in water potential from soil-to-root, which lowers ψ_{root}, decreasing the amount of HR.Therefore, in PHS, more HR occurs at night, in accordance with observations and theory [*Oliveira et al.*, 2005; *Lee et al.*, 2005].

HR is predominately downwards during the wet season (FMA), serving to diminish the gradient between the newly-wetted surface and still-dry depths (Supp Figs A.6,A.7). Redistribution occurs in both directions during the dry season (SON), downwards after rain events, and upwards with drying. Only with TFE, and only during the dry season, is there significant extraction beyond 6 meters (Figs 8, 9). There is very little water deposited at depths beyond 6 meters at any point in either simulation.

Under ambient conditions simulated HR in PHS totals to 41.3 cm (10.3 cm during the day, 31.0 cm at night), Figure 9. HR declines slightly to 37.0 cm (11.5 cm day and 25.5 cm night) with TFE. For reference, total transpiration over the same time period was 120 and 99 cm for ambient and TFE conditions, respectively. The TFE simulation has less HR overall, but more HR during wet months, Feb-June.

Increased downwards? HR within the TFE plot occurs in Feb-June, associated with the drier TFE soils and larger gradients in soil potential from surface to depth. HR is lower in January, and July-December with TFE. Similar to during the wet months the gradient in soil potential (in this case from depth to surface) is larger with TFE. However, the soils overall are so dry with TFE during the dry months, that loss of conductance from soil-to-root counteracts the large gradient, resulting in lower HR.

The dynamics of HR with PHS align with observations, with more HR at night, and HR occurring in both directions vertically [*Burgess et al.*, 1998]. The absolute values of HR are difficult to assess, given limited observations.

In PHS, Allowing HR to occur into the top layer of the soil column significantly degraded modeled soil evaporation (not shown). We opted to omit the first top Layer (spanning 0 to 2 cm below ground) soil-to-root hydraulic conductance, to prevent HR from oversupplying water for soil evaporation.

6.6.1 Is hydraulic redistribution a feature or a liability?

HR is a natural consequence of using Darcy's Law to model root water uptake - when hydraulic gradients are reversed, HR should occur. As such it is naturally included within a plant hydraulics model with multiple soil layers and is an emergent behavior of respecting hydraulic flow down gradient of potentials. In ESMs, where soil moisture is typically

resolved vertically, interfacing the plant hydrulics with a multi-layer soil naturally accounts for HR. Other models, similar to the SMS paradigm, disallow HR by constraining root water uptake to be positive [*Xu et al.*, 2016].

Most literature models force the model with a single bulk soil water potential ψ_s, which precludes HR [*Fisher et al.*, 2007; *Bonan et al.*, 2014; *Sperry et al.*, 2017]. *Christoffersen et al.* [2016] expand beyond a single ψ_s horizontally, representing soil elements at different charecteristic distances from the root surface, but still feature a single soil layer in the vertical dimension.

Likewise HR is likely sensitive to the representation of vegetation tissue capacitance and below-ground hydraulic segmentation (CITAIONS NEEDED).

Hydraulic redistribution has the impact of reducing the variance in the availability of water for plant transpiration, potentially at odds with observations of interannual variation (see Lawrence et al in prep. Tang et al. 2015) Observations of HR are extremely difficult, in unequivocal detection of HR involves the observation of reverse flow along transport roots, typically at rates close ot the detection threshold of sap flow monitoring systems. Therefore, the degree to which HR actually occurs in unclear. While there is some first-order benefit to plants of moving water from deep soil to surface layers to allow more transpiration, this water is then also available for competition with other shallow-rooted plants, and for evaporative processes. Further, cavitation of fine roots in shallow soils might explicitly act as a 'fuse' to prevent loss of water from the plant into dry soil layers (Kotowska et al. 2015) - a process not explicitly resolved here. Therefore we view this first implementation of HR into the default versions of the CLM as a 'null' hypothesis for the functioning of this process, and as a platform to allow further refinement from the plant hydraulics community.

6.7 Soil moisture profile

The column total soil water in all four simulations is initialized at 2.66 meters (over an 8.6-meter soil column) (SAY WHY). The change in total soil water is small under ambient conditions, decreasing by 0.3cm with PHS and 9.6cm with SMS over the three-year simulations. Root zone soil potential is lower with SMS, with a root-fraction-weighted average soil potential of -0.42 MPa during November 2003. The equivalent metric from PHS, average predawn root water potential, is -0.08 MPa.

Under 60% through-fall exclusion, the change in soil water is -1.12 meters with PHS and -0.94 meters with SMS, relative to the ambient simulations (Supp Fig A.11).

With SMS, root-fraction-weighted average soil potential is -2.18MPa during November 2003, whereas PHS average predawn root water potential is -0.37MPa (Figure 10). Observations of root-zone potential based on gravity-corrected predawn leaf water potential are -0.17 +/- 0.10 MPa under ambient conditions, and -0.71 +/- 0.31 MPa with through-fall exclusion (also in November 2003) [*Fisher et al.*, 2007]. The SMS root-weighted water potential is 1.81 MPa drier (from a soil water potential perspective) because the SMS continues to extract water from dry layers with high fractions of roots, further drying these layers and decreasing the root-weighted water potential (see Section 6.4). Further, PHS has more access to deep soil water under dry conditions (Fig 7), which mitigates declines in soil potential near the surface.

While PHS better matches observations of root-zone soil potential, we hesitate to make conclusions about model skill due to parameter uncertainty and due to the fact that these values may be sensitive to tuning (see Section 4.1), as well as the fact that both models feature high biases in transpiration relative to observations.

Darcy's Law establishes that water flow is proportional to the gradient in total water potential. With PHS, this gradient is measured relative to dynamic ψ_{root}. With SMS, this gradient is measured relative to a constant parameter, ψ_c, the soil water potential at which

stomates fully close. This approach is required without prognostic vegetation water potential, but yields unsatisfactory dynamics that do not comply with the physics of porous media flow (see Section 6.4). Furthermore, it seems that ψ_c has historically been tuned for its effects on diffusive fluxes, without specific attention to the effect on soil moisture dynamics (Can someone else back me up on this? Is there a way to cite this?).

This is problematic because soil moisture dynamics are very sensitive to ψ_c. Root water uptake halts when soil potential reaches ψ_c (Section 3), setting an effective minimum soil potential, a situation that is apparent in Figure 10 where soil water potential for SMS stays at approximately -2.5 MPa, which is the value of ψ_c for evergreen tropical broadleaf trees (?. This feature is clearer in Figure A.13, where soil layers can be seen to dry out quickly, but not beyond -2.5 MPa (with the exception of Soil Layers 1 and 2, which are influenced by bare soil evaporation). The effect of ψ_c extends to ambient through-fall conditions (Fig A.12), but over a smaller spatial and temporal domain. PHS has more flexibility, due to dynamic root water potential, so there is not the same tendency to dry out quickly to a specific level. Instead minimum soil water potential for PHS gets lower each dry season throughout the TFE simulation (Fig 10a).

[Add some material looking at the vertical profile of soil moisture in the models vs observations?]

Soil water dynamics in CLM are sensitive to the representation of root water uptake, but due to the scarcity of observational constraints, vertically-resolved soil moisture predictions are challenging to evaluate.

With PHS, because we're modeling vegetation water potential, we can utilize a hydraulic framework, which offers a well-established physical basis and a clear improvement in model structure. SMS root water uptake has problematic model structure, seemingly no empirical basis, and intuitively does not look good on soil water dynamics. PHS improves model structure, but it also adds parameters that are difficult to constrain.

PHS offers leaf and stem water potential observations, which are downstream of soil potential, and could be an exciting opportunity to interface with observations. While PHS seems a clear improvement over SMS, which does not comport well with fundamental aspects of hydraulic theory, further work on the representation of root water uptake in models is needed to validate both soil water states and fluxes.

7 Conclusion

7.1 Caveats

Modeling stomatal conductance and photosynthesis, especially subject to water stress, is an area of ongoing research. We use the Medlyn model coupled to a hydraulic stress function that attenuates V_{cmax}. This complies with observations [*Lin et al.*, 2018; *Zhou et al.*, 2013] that stress applied through g_1 underestimates attenuation of photosynthesis. However, there is no direct evidence of declines in V_{cmax} with drought [*Flexas et al.*, 2006], whereby future work may seek to represent mesophyll conductance in CLM.

The model hydraulic supply representation is simplified, to reduce the model parameter and computational burdens. No capacitance. No integration of xylem or soil conductances vulnerability, instead based on lower node. No hysteresis in loss of conductance, xylem instantly regain conductance upon re-wetting. Leaf conductance simplified. Soil layers fully parallel, soil potential constant each time step.

Parameter uncertainty is significant. Notions of hydraulic architecture will never perfectly fit on this modeling scale, especially in a PFT paradigm. Field measurements of hydraulic traits will help constrain parameter ranges, but mostly only aboveground. Flux observations can help to tune stress parameters. Parameter estimation for root functioning is

significantly more challenging, given the difficulty in underground trait observations. Likewise observational constraints of vertically-resolved states and fluxes underground are scarce. Follow-up work will be geared towards parameter estimation and assessing model skill.

7.2 Utility of modeling vegetation water potential

The PHS configuration of the CLM5 is, to our knowledge, the first Earth System Model with a representation of plant water potential running in its default configuration. In this paper, we have described the model implementation, and illustrated a comparison of the model dynamics for a tropical rainforest site subjected to water limitation, given that prediction of rainforest responses to drought is one of the key uncertainties in the ESM predictions. Overall, the new model behaviour differs from the default configuration in ways that are expected, given its structural properties, and in many cases, provides better correspondance with the observations that the default structure.

In this paper, however, we do not undertake a comprehensive assessment of which model structure performs better, given the substantial parametric uncertainty in both models, and the dependence on numerous other features of the CLM external to water stress representation that contribute to model-observation divergences - in this case in particular, the overestimation of unstressed transpiration by both versions of the model compared to the observations.

In lieu of this type of assessment, we propose that the new PHS model structure 1) is more closely aligned with known plant hydraulics theory, 2) provides significantly improved connections to real-world observational data streams (of leaf and stem water status, sap flow, percent loss conductance) and 3) represents known features of ecohydrological function that the default model cannot capture, including hydraulic redistribution, changes in the depth of water uptake with drought stress, plant embolism impacts on gas exchange and responses of water uptake to changes in leaf:root rations.

This will be the final conclusions. Any comments on overall takeaways?

PHS models vegetation water potential. This offers structural improvements for stress and for root water uptake. Stress now functions with hydraulic limitation.

8 Acknowledgments

9 Figures

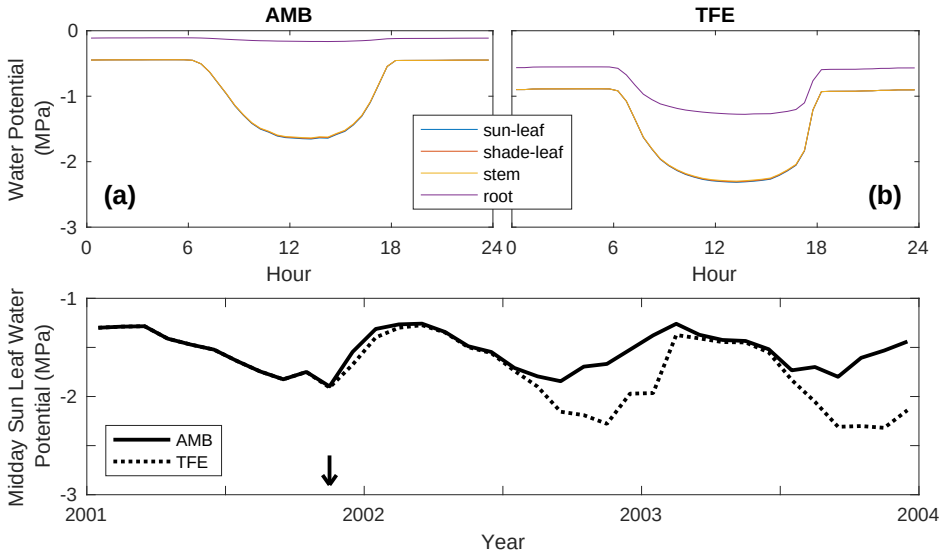

Figure 2. Modeled vegetation water potential at Caxiuanã, Brazil. (a) 2003 Dry season (SON) diurnal mean, ambient through-fall conditions, (b) 2003 Dry season (SON) diurnal mean, with 60% through-fall excluded. Curves are drawn for sunlit leaf, shaded leaf, stem, and root water potentials. Note that the first three mostly overlap. (c) Monthly mean midday leaf water potential, under ambient (solid line) and 60% through-fall exclusion (dotted line) conditions. Note that through-fall exclusion begins in month 11 (Nov 1, 2001).

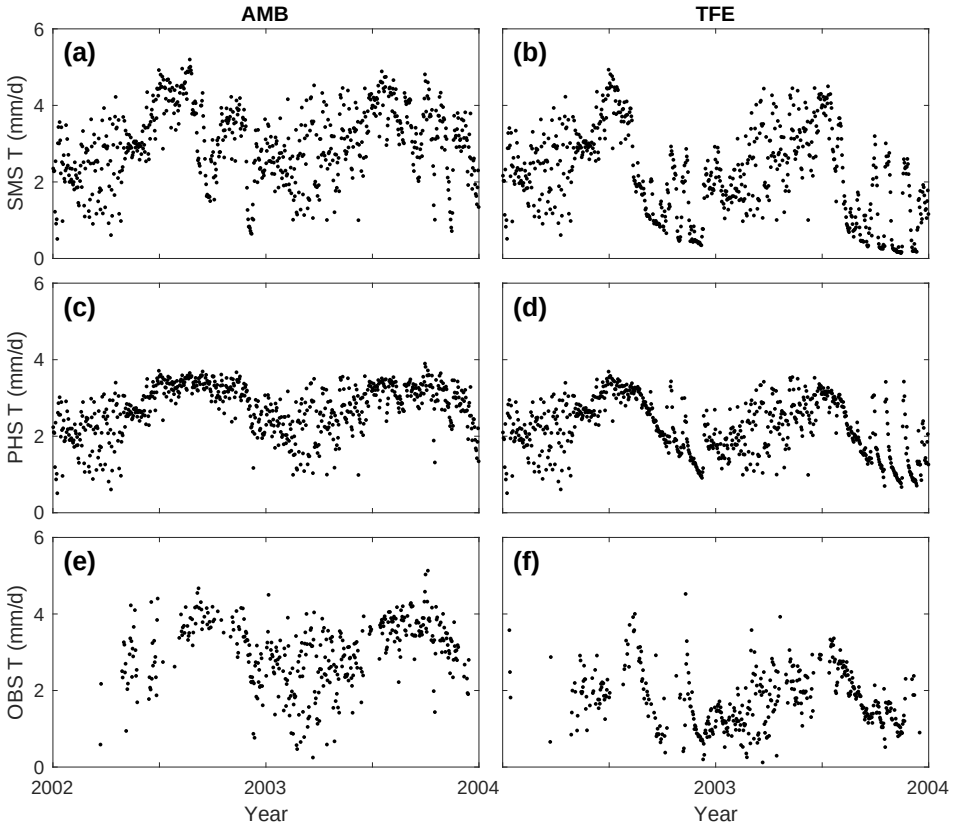

Figure 3. (a,b) Monthly mean water stress function. Note that the water stress function equals 1 when there is no stress and 0 when fully stressed. (c,d) Monthly mean transpiration (W/m^2). (e,f) Monthly mean gross primary productivity ($g/m^2/d$). Solid lines correspond to ambient through-fall conditions, and dotted lines feature 60% through-fall exclusion. Black lines represent model output. Red lines show observational transpiration derived from sap flux (see zqz). PHS is on for (a), (c), and (e). PHS is off for (b), (d), and (f).

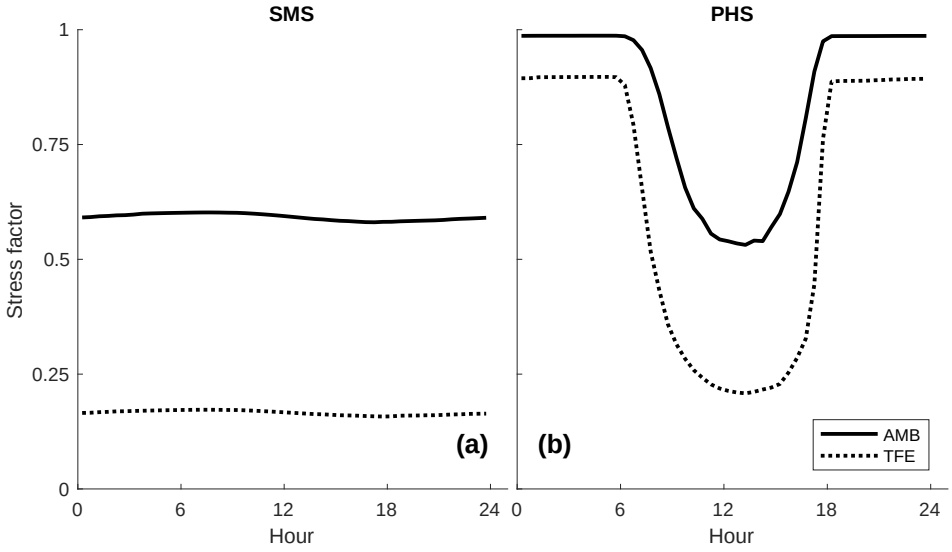

873 **Figure 4.** 2003 Dry season (SON) diurnal mean water stress function for (a) PHS off, and (b) PHS off.
874 Solid lines correspond to ambient through-fall conditions, and dotted lines feature 60% through-fall exclusion.
875 Note that the water stress function equals 1 when there is no stress and 0 when fully stressed.

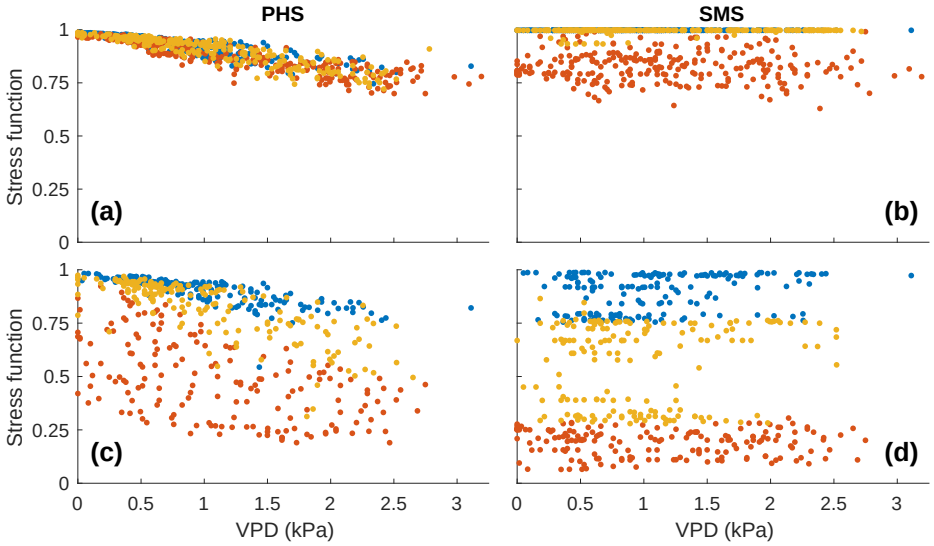

Figure 5. Water stress function versus vapor pressure deficit, for points with downwelling shortwave radiation between 400 and 425 W/m2. (a) PHS, ambient through-fall (b) SMS, ambient through-fall (c) PHS, 60% through-fall excluded (d) SMS, 60% through-fall excluded. For (a) and (c) data are subdivided based on predawn root water potential. For (b) and (d) data are subdivided based on average soil matric potential, weighted by root fraction. Blue dots represent the wettest tercile, yellow dots represent the intermediate tercile, and red dots represent the driest tercile. Note that panels (c) and (d) exclude data from 2001, when CO_2 exclusion was not active.

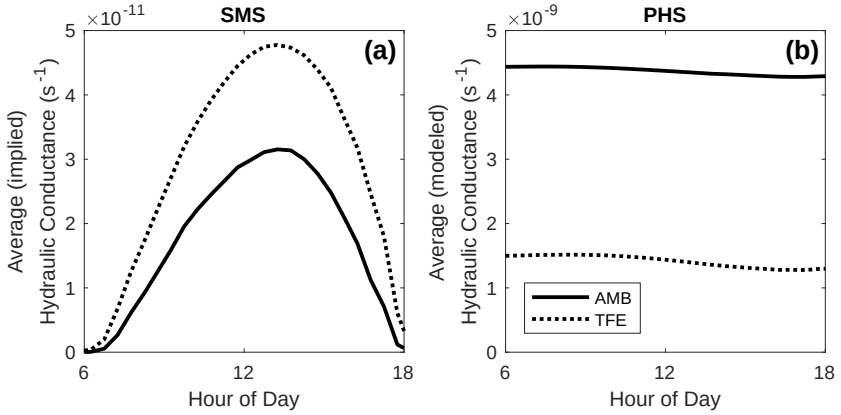

Figure 6. Soil Layer 3 conductance, under ambient through-fall conditions in 2003. (a) Time-series of PHS modeled soil-to-root conductance (s^{-1}) from Soil Layer 3 (spanning 6 to 12 centimeters in depth). (b) Time-series of SMS inferred conductance (s^{-1}) also from Soil Layer 3. (c) Concurrent precipitation forcing (mm/d).

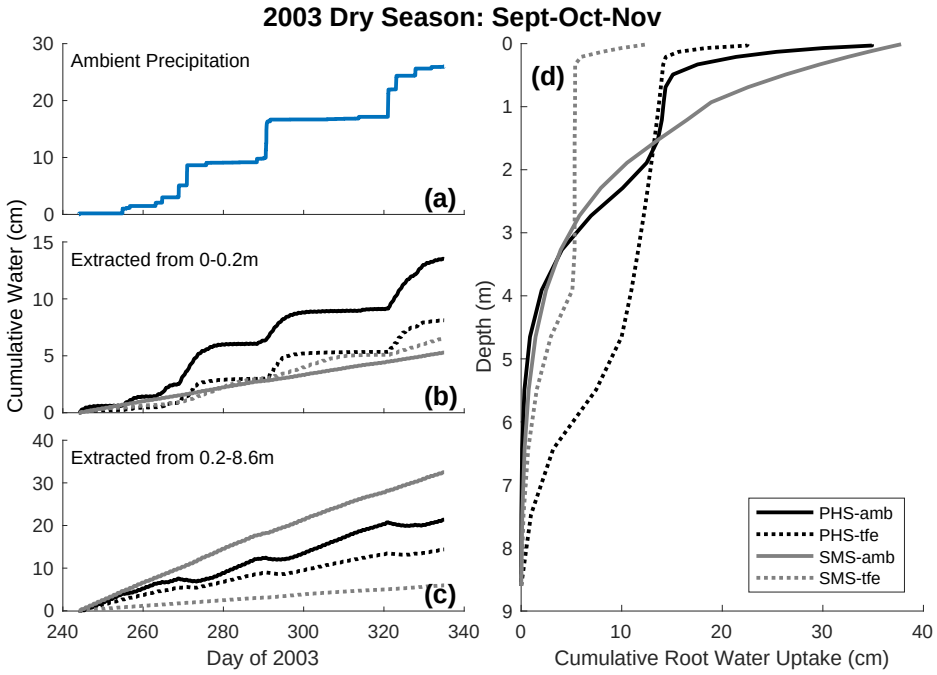

Figure 7. 2003 dry season (SON) cumulative root water uptake and precipitation. (a) Cumulative root water uptake with depth across the four simulations. (b,c) Cumulative water uptake over time from above and below 0.2m, respectively. (d) Cumulative precipitation under ambient conditions.

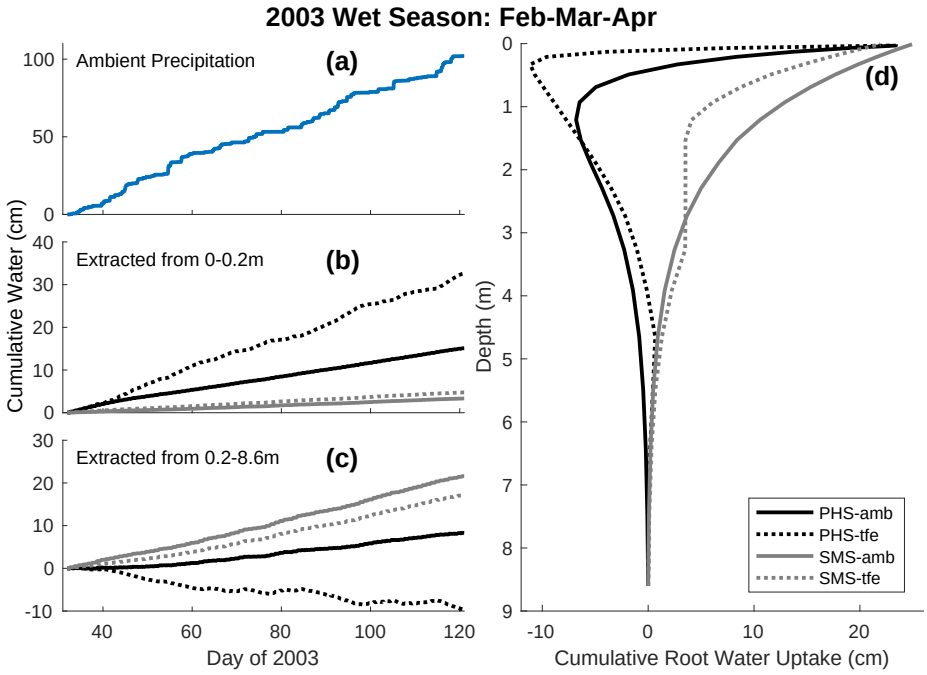

Figure 8. 2003 wet season (FMA) cumulative root water uptake and precipitation. (a) Cumulative root water uptake with depth across the four simulations. (b,c) Cumulative water uptake over time from above and below 0.2m, respectively. (d) Cumulative precipitation under ambient conditions.

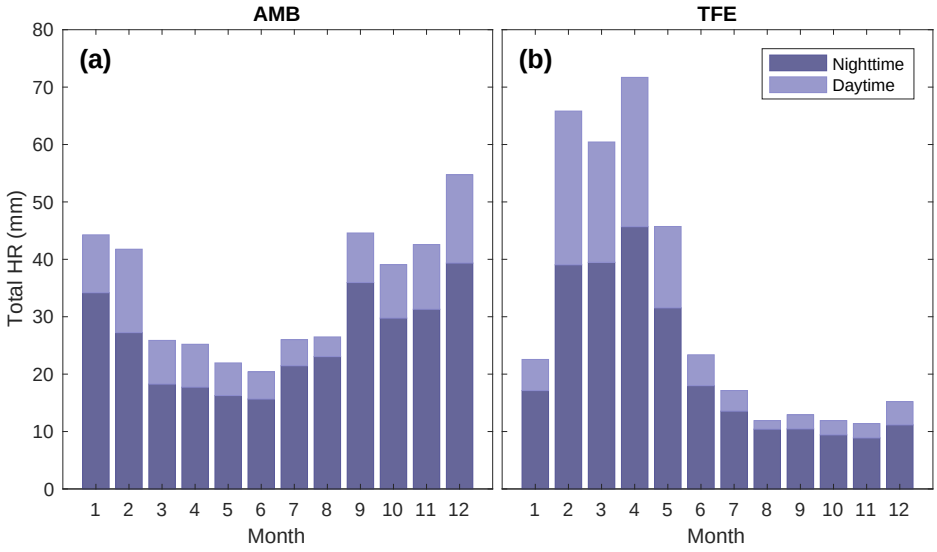

Figure 9. Total hydraulic redistribution (mm) by month in 2003. For (a) ambient through-fall conditions, and (b) 60% through-fall exclusion. Darker shading shows portion of HR at night [6pm,6am), lighter shading shows portion of HR during day [6am,6pm).

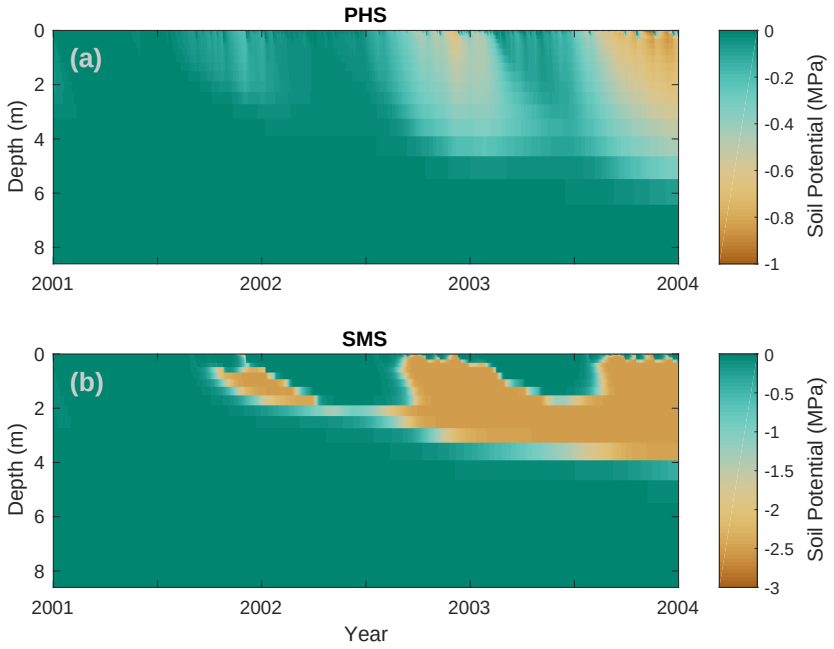

Figure 10. Vertical profile of soil water potential (MPa) over time under 60% through-fall exclusion, for (a) PHS, and (b) SMS. Note that color axes are different.

898 # A: Supplementary Figures

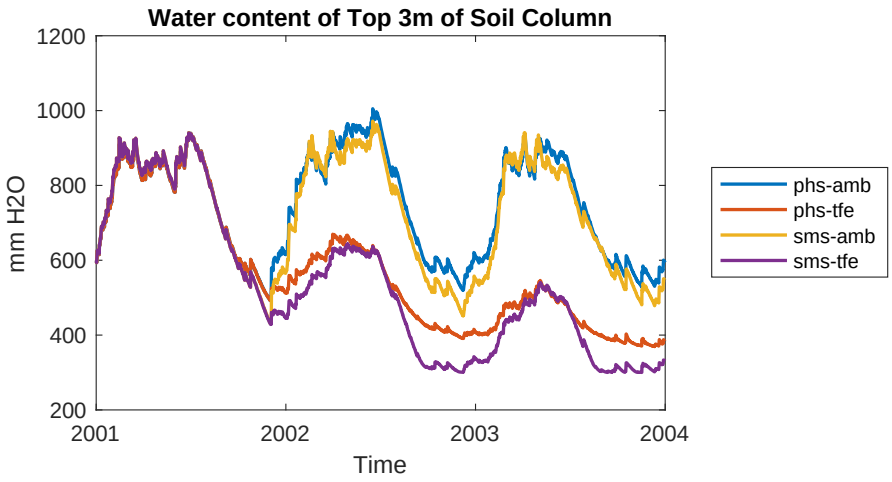

899 **Figure A.1.** Total water content of the top three meters of the soil column through time for the four simula-
900 tions.

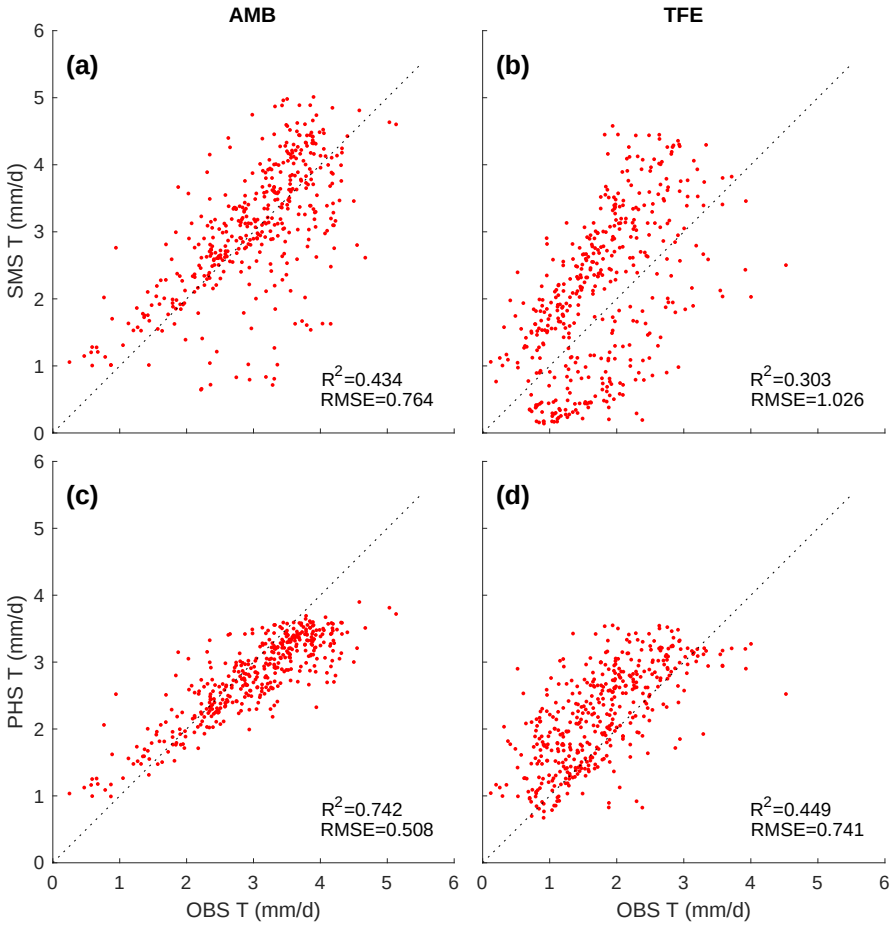

901 **Figure A.2.** Total water content of the top three meters of the soil column through time for the four simula-
902 tions.

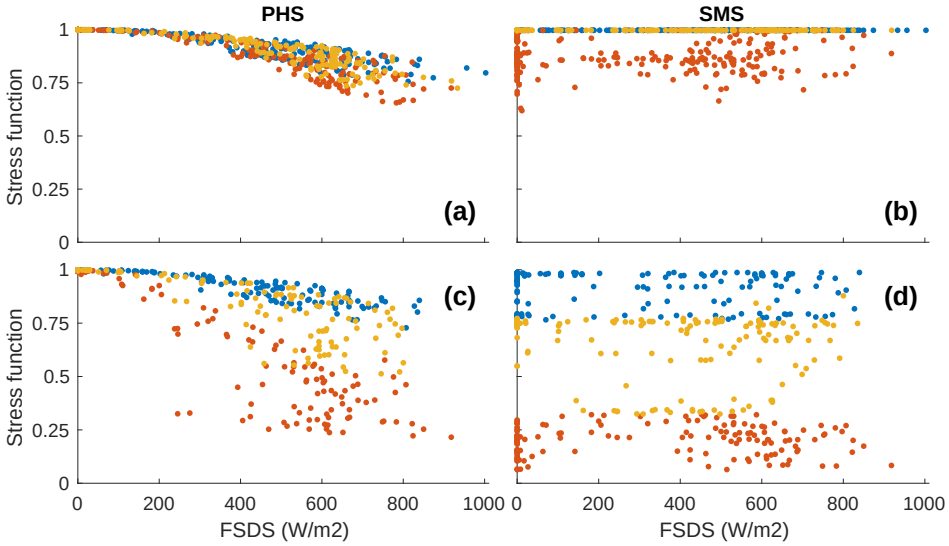

Figure A.3. Water stress function versus downwelling shortwave radiation for points with vapor pressure deficit between 1 and 1.0559 kPa. (a) PHS, ambient through-fall (b) SMS, ambient through-fall (c) PHS, 60% through-fall excluded (d) SMS, 60% through-fall excluded. For (a) and (c) data are subdivided based on predawn root water potential. For (b) and (d) data are subdivided based on average soil matric potential, weighted by root fraction. Blue dots represent the wettest tercile, yellow dots represent the intermediate tercile, and red dots represent the driest tercile. Note that panels (c) and (d) exclude data from 2001, when through-fall exclusion was not active.

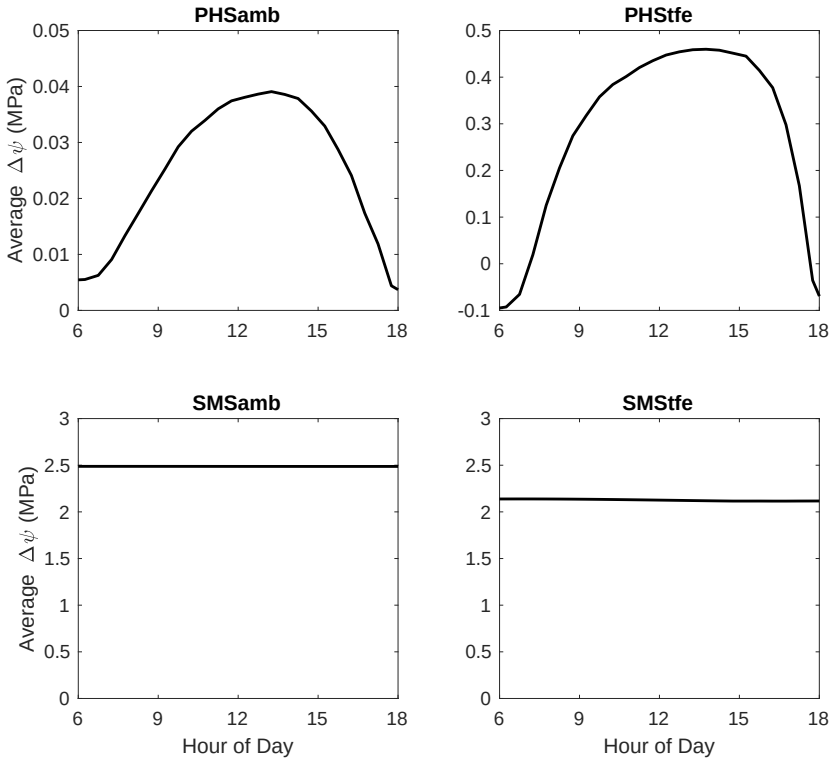

Figure A.4. To complement Figure 6

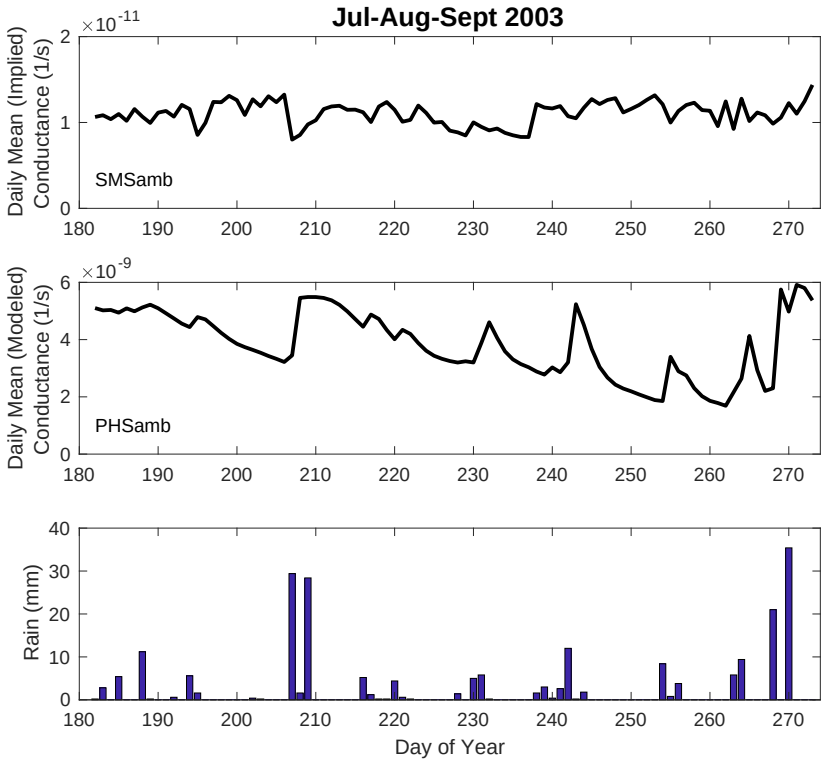

Figure A.5. May be better captured by next figure

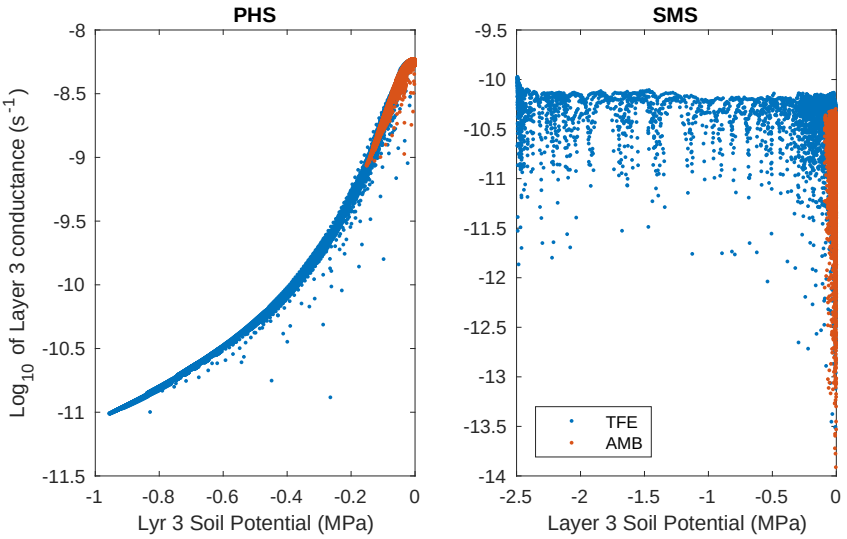

912 **Figure A.6.** Log of conductance versus soil potential for Soil Layer 3 (2003).

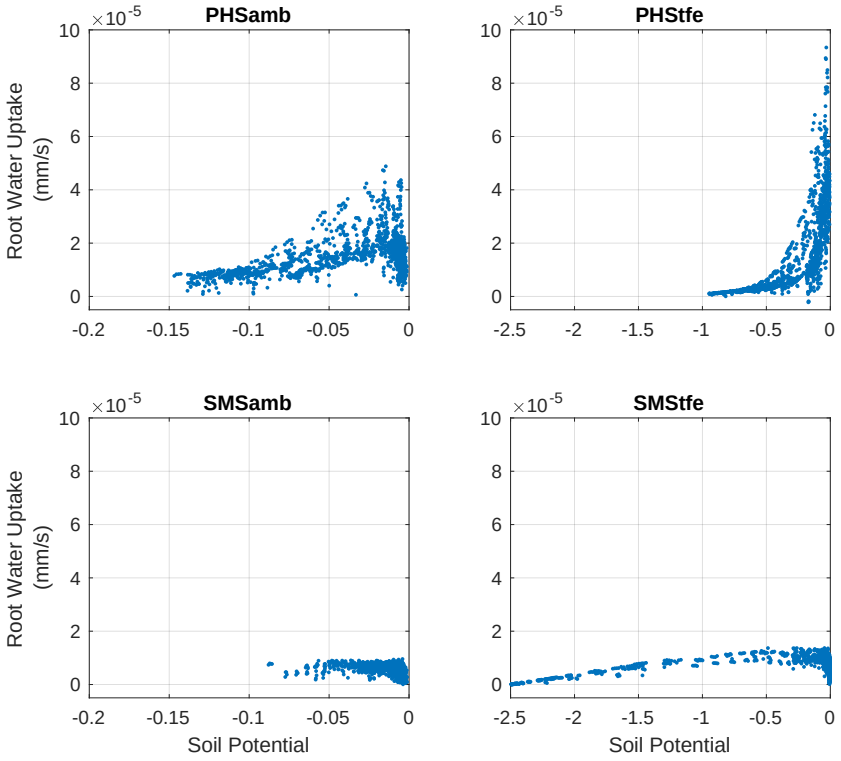

Figure A.7. Midday root water uptake versus soil potential for Soil Layer 3 (2003).

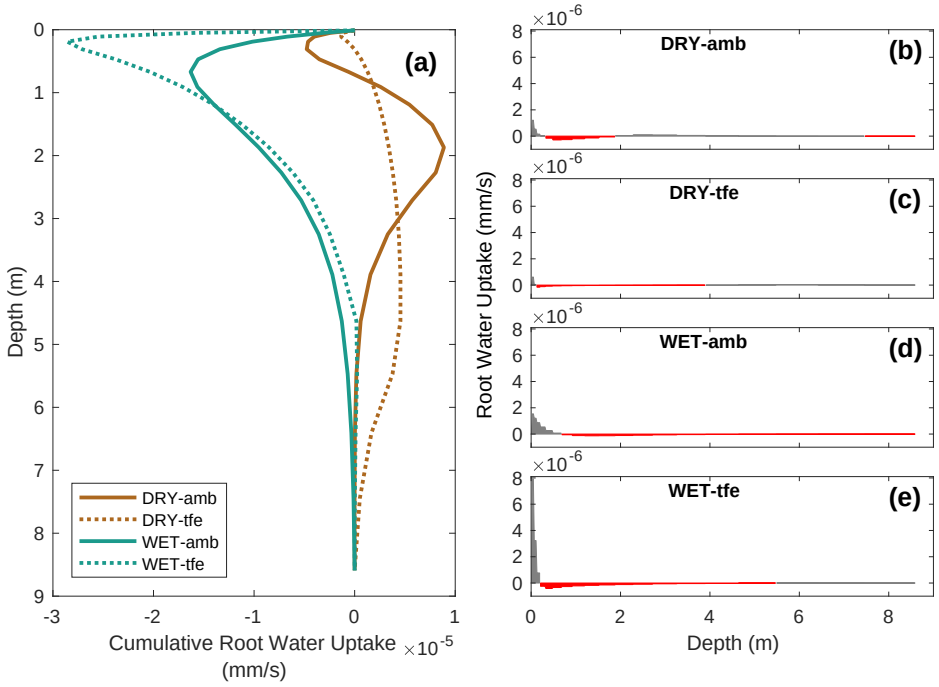

Figure A.8. PHS, nighttime (6pm to 6am) average root water uptake profiles with depth. Showing nighttime serves to emphasize the profile of hydraulic redistribution. Panel (a) shows cumulative (starting at depth) root water uptake (mm/s) for ambient (solid line) and 60% through-fall exclusion (dotted line) during the wet (FMA, cyan color) and dry (SON, brown color) seasons. Panels (b)-(e) present the information from (a) in non-cumulative form. Note that for panels (b)-(e) negative root water uptake is shaded red, and also that for panel (a), positive slope indicates water uptake, and negative slope indicates water deposited. Note also that SMS is not shown, because hydraulic redistribution is precluded.

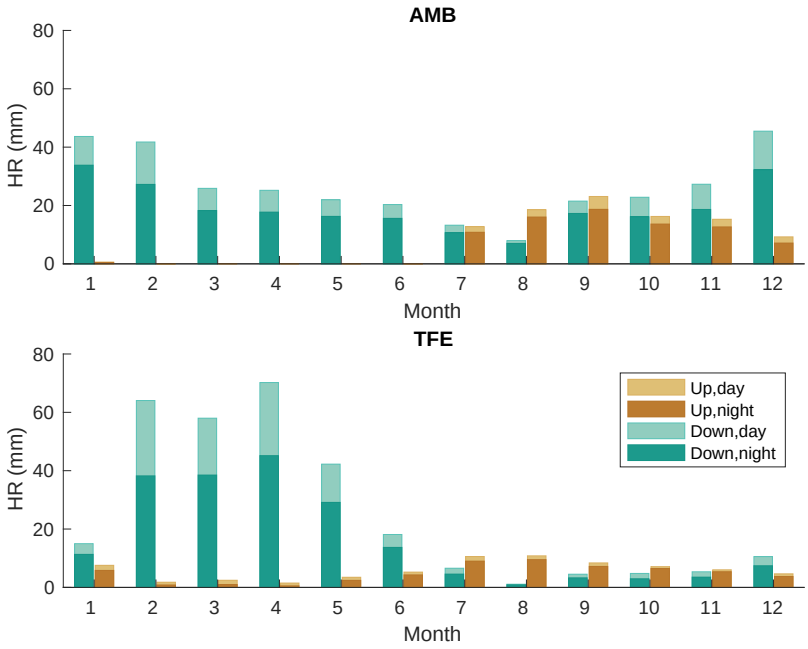

Figure A.9. PHS hydraulic distribution during 2003. Alternative version partitioning by direction.

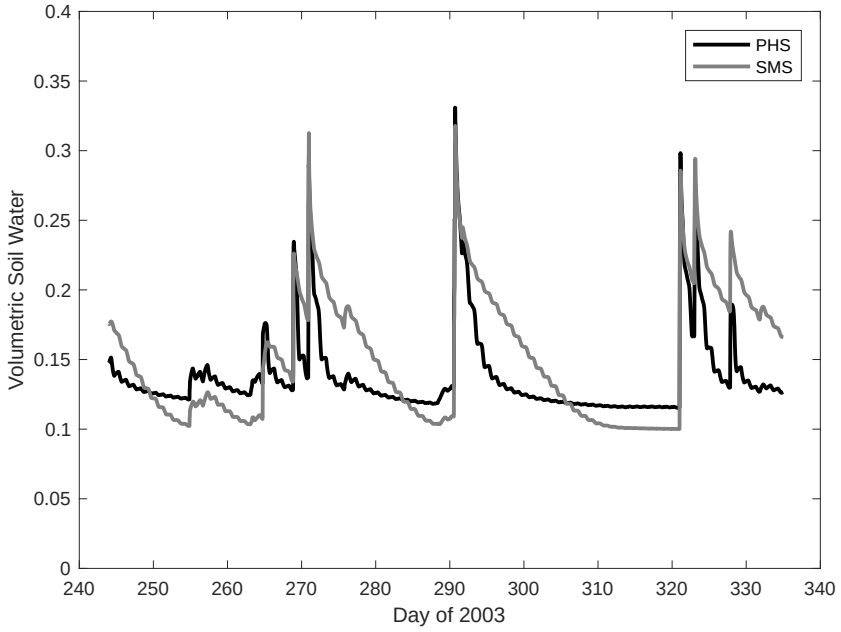

Figure A.10. Volumetric soil water content in Soil Layer 2 (which spans 2-6cm in depth), for SON-2003, featuring 60% through-fall exclusion. With PHS (black line), the soil layer can dry out much more quickly after rain events.

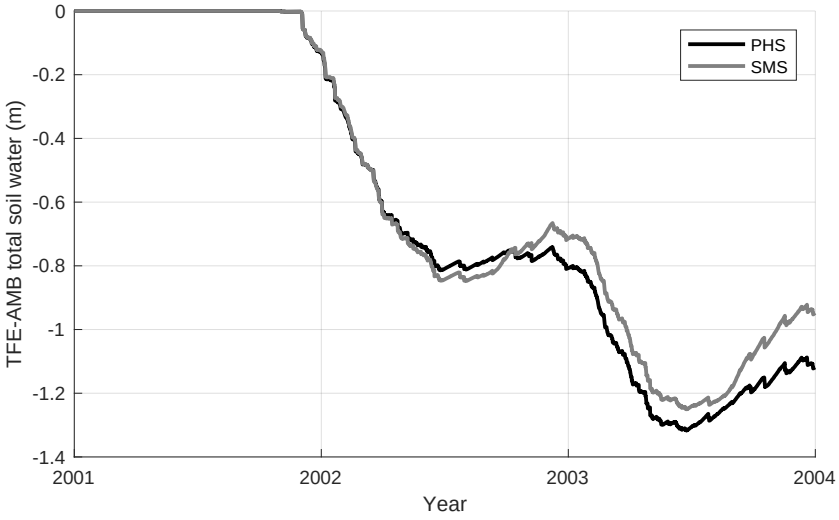

925 **Figure A.11.** Delta soil water

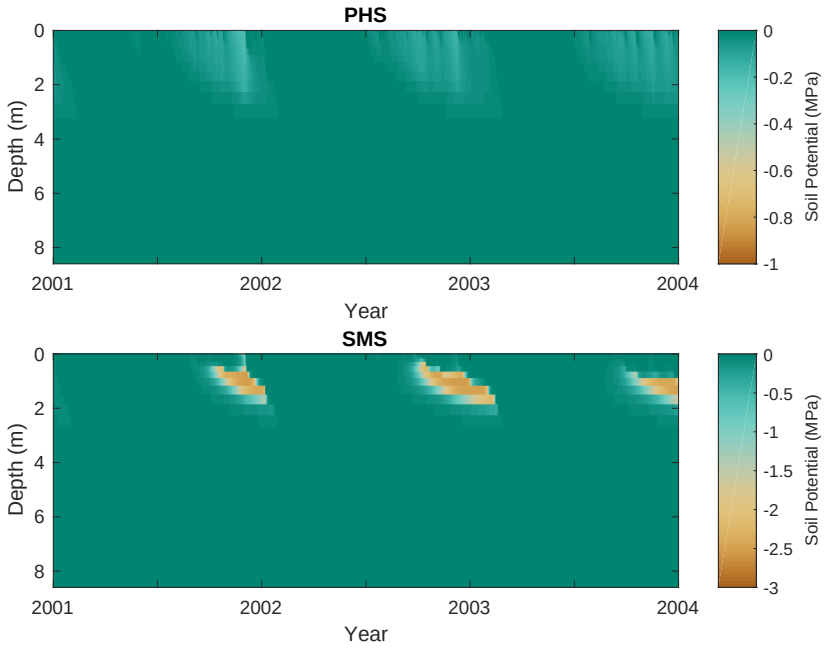

926 **Figure A.12.** Vertical profile of soil water potential (MPa) through time under ambient through-fall condi-
927 tions, for (a) PHS, and (b) SMS. Note that color axes are different.

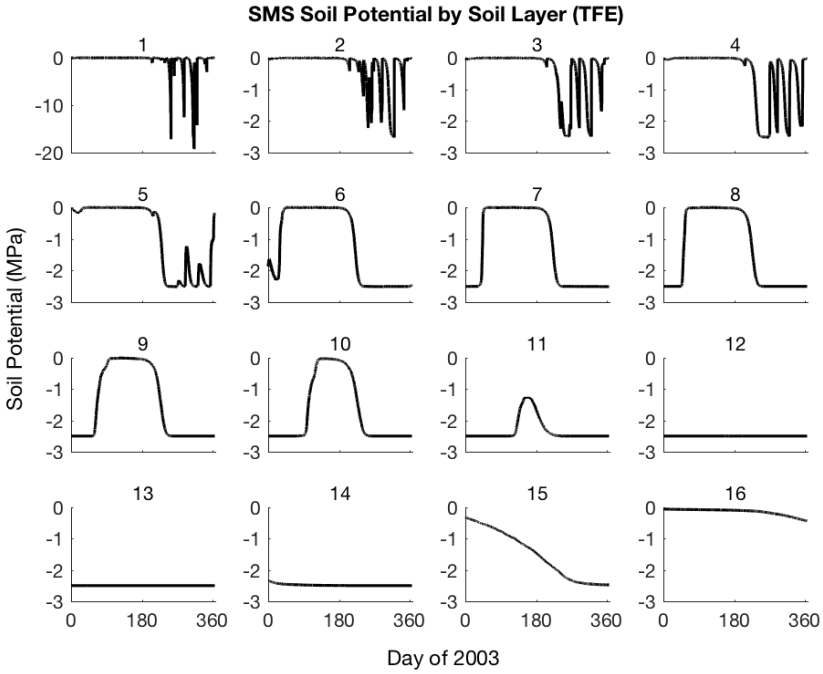

Figure A.13. Time series of soil potential by soil layer, with SMS, under 60% through-fall exclusion. This duplicates the information in Figure 10a to highlight the the sensitivity of soil moisture dynamics to the SMS parameter, ψ_c (soil potential with stomates fully closed, -2.5 MPa). Soil Layers 17-20, which do not dry out completely (similar to Soil Layer 16), are not shown.

B: Appendix to Model Description

B.1 Details of Water Supply

PHS resolves flow across four different segments, soil-to-root, root-to-stem, stem-to-leaf, and leaf-to-transpiration.

Stem-to-leaf. The area bases are sunlit and shaded leaf area, respectively. Note that gravity is assumed negligible here. Likewise there is no length scaling applied to maximum conductance. Therefore the input parameters for $k_{1,\max}$ should be conductances (s^{-1}).

$$\begin{aligned} q_{1a} &= k_1 \cdot \text{LAI-sun} \cdot (\psi_{\text{stem}} - \psi_{\text{sun-leaf}}) \\ q_{1b} &= k_1 \cdot \text{LAI-shade} \cdot (\psi_{\text{stem}} - \psi_{\text{shade-leaf}}) \end{aligned} \tag{B.1}$$

$$k_1 = k_{1,\max} \cdot f\left(\psi_{\text{stem}}\right) \tag{B.2}$$

$$f\left(\psi\right) = 2^{-\left(\frac{\psi}{p_{50}}\right)^{c_k}} \tag{B.3}$$

Root-to-stem. The area basis is stem area index. The parameter is maximum stem xylem conductivity ($K_{2,\max}$). Stem conductance (k_2) is the result of scaling maximum conductivity by the tree height (h) and applying loss relative to maximum conductance via the vulnerability curve $f\left(\psi_{\text{root}}\right)$.

$$q_2 = k_2 \cdot \text{SAI} \cdot (\psi_{\text{root}} - \psi_{\text{stem}} - \rho g h) \tag{B.4}$$

$$k_2 = \frac{K_{2,\max}}{h} \cdot f\left(\psi_{\text{root}}\right) \tag{B.5}$$

Soil-to-root. Area basis is RAI in soil layer i, which is based on the layer root fraction times the total root area. Total root area we have as the summed stem and leaf area indices multiplied by a relative root area parameter (f_{root}). The vertical root distribution is defined by the layer root fraction (r_i), which follows a one-parameter (by PFT) power law decay following *Jackson et al.* [1996].

$$q_{3,i} = k_{3,i} \cdot \text{RAI}_i \cdot (\psi_{\text{soil,i}} - \psi_{\text{root}} - \rho g z_i) \tag{B.6}$$

$$\text{RAI}_i = f_{\text{root}} \cdot (\text{SAI} + \text{LAI}) \cdot r_i \tag{B.7}$$

$$k_{3,i} = \frac{k_{r,i} + k_{s,i}}{k_{r,i} \cdot k_{s,i}} \tag{B.8}$$

$$k_{r,i} = \frac{K_{r,\max}}{l_i} f\left(\psi_{\text{soil,i}}\right) \tag{B.9}$$

$$l_i = z_i + x \tag{B.10}$$

$$k_{s,i} = \frac{K_{s,i}}{d} \tag{B.11}$$

The conductance $k_{3,i}$ reflects two resistors in series, from soil-to-root ($k_{s,i}$) and through the root tissue ($k_{r,i}$). The root tissue conductance is attenuated via the vulnerability curve framework. The input parameter is maximum root xylem conductivity, on the basis of RAI as defined above. The root conductivity is scaled by the conducting length, which is estimated as the sum of soil layer depth (z_i) and average lateral extent (x, static parameter). The soil conductivity $K_{s,i}$ is calculated from the layer soil matric potential (ψ_s) and soil properties following *Clapp and Hornberger* [1978] as described in *Oleson et al.* [2013]. The soil conductance ($k_{s,i}$) is the result of scaling the conductivity by d, the distance between roots estimated following *Williams et al.* [1996] and *Bonan et al.* [2014]

The challenge here is obviously getting your head around all the parameters.

B.2 Details of Water Demand

B.3 Details of Solution

The continuity of water flow through the system yields four equations

$$\begin{aligned} E_{sun} &= q_{1a} \\ E_{shade} &= q_{1b} \\ q_{1a} + q_{1b} &= q_2 \\ q_2 &= \sum_{i=1}^{nlevsoi} q_{3,i} \end{aligned} \tag{B.12}$$

We seek the set of vegetation water potential values (four unknowns),

$$\psi = \begin{bmatrix} \psi_{sunleaf} \\ \psi_{shadeleaf} \\ \psi_{stem} \\ \psi_{root} \end{bmatrix} \tag{B.13}$$

that satisfies these equations, as forced by the soil moisture and atmospheric state.

Each flux on the schematic can be represented in terms of the relevant water potentials.

Defining the transpiration fluxes:

$$\begin{aligned} E_{sun} &= E_{sun,max} \cdot 2^{-\left(\frac{\psi_{sunleaf}}{p50_e}\right)^{c_k}} \\ E_{shade} &= E_{shade,max} \cdot 2^{-\left(\frac{\psi_{shadeleaf}}{p50_e}\right)^{c_k}} \end{aligned} \tag{B.14}$$

Defining the water supply fluxes:

$$\begin{aligned} q_{1a} &= k_{1a,max} \cdot 2^{-\left(\frac{\psi_{stem}}{p50_1}\right)^{c_k}} \cdot \mathrm{LAI}_{sun} \cdot \left(\psi_{stem} - \psi_{sunleaf}\right) \\ q_{1b} &= k_{1b,max} \cdot 2^{-\left(\frac{\psi_{stem}}{p50_1}\right)^{c_k}} \cdot \mathrm{LAI}_{shade} \cdot \left(\psi_{stem} - \psi_{shadeleaf}\right) \\ q_2 &= \frac{k_{2,max}}{z_2} \cdot 2^{-\left(\frac{\psi_{root}}{p50_2}\right)^{c_k}} \cdot SAI \cdot (\psi_{root} - \psi_{stem} - \Delta\psi_z) \\ q_{soil} &= \sum_{i=1}^{nlevsoi} q_{3,i} = \sum_{i=1}^{nlevsoi} k_{3,i} \cdot RAI \cdot (\psi_{soil,i} - \psi_{root} + \Delta\psi_{z,i}) \end{aligned} \tag{B.15}$$

We're looking to find the vector ψ that fits with soil and atmospheric forcings while satisfying water flow continuity. Due to the model non-linearity, we use a linearized explicit approach, iterating with Newton's method. The initial guess is the solution for ψ (vector) from the previous time step. The general framework, from iteration m to $m + 1$ is:

$$\begin{aligned} q^{m+1} &= q^m + \frac{\delta q}{\delta \psi}\Delta\psi \\ \psi^{m+1} &= \psi^m + \Delta\psi \end{aligned} \tag{B.16}$$

So for our first flux balance equation, at iteration $m + 1$, we have:

$$E_{sun}^{m+1} = q_{1a}^{m+1} \tag{B.17}$$

Which can be linearized to:

$$E_{sun}^{m} + \frac{\delta E_{sun}}{\delta \psi}\Delta\psi = q_{1a}^{m} + \frac{\delta q_{1a}}{\delta \psi}\Delta\psi \tag{B.18}$$

And rearranged to be:

$$\frac{\delta q_{1a}}{\delta \psi}\Delta\psi - \frac{\delta E_{sun}}{\delta \psi}\Delta\psi = E_{sun}^{m} - q_{1a}^{m} \tag{B.19}$$

And for the other 3 flux balance equations:

$$\begin{aligned} \frac{\delta q_{1b}}{\delta \psi}\Delta\psi - \frac{\delta E_{sha}}{\delta \psi}\Delta\psi &= E_{sha}^{m} - q_{1b}^{m} \\ \frac{\delta q_{2}}{\delta \psi}\Delta\psi - \frac{\delta q_{1a}}{\delta \psi}\Delta\psi - \frac{\delta q_{1b}}{\delta \psi}\Delta\psi &= q_{1a}^{m} + q_{1b}^{m} - q_{2}^{m} \\ \frac{\delta q_{soil}}{\delta \psi}\Delta\psi - \frac{\delta q_{2}}{\delta \psi}\Delta\psi &= q_{2}^{m} - q_{soil}^{m} \end{aligned} \tag{B.20}$$

Putting all four together in matrix form:

$$\begin{bmatrix} \frac{\delta q_{1a}}{\delta \psi} - \frac{\delta E_{sun}}{\delta \psi} \\ \frac{\delta q_{1b}}{\delta \psi} - \frac{\delta E_{sha}}{\delta \psi} \\ \frac{\delta q_{2}}{\delta \psi} - \frac{\delta q_{1a}}{\delta \psi} - \frac{\delta q_{1b}}{\delta \psi} \\ \frac{\delta q_{soil}}{\delta \psi} - \frac{\delta q_{2}}{\delta \psi} \end{bmatrix} \Delta\psi = \begin{bmatrix} E_{sun}^{m} - q_{1a}^{m} \\ E_{sha}^{m} - q_{1b}^{m} \\ q_{1a}^{m} + q_{1b}^{m} - q_{2}^{m} \\ q_{2}^{m} - q_{soil}^{m} \end{bmatrix} \tag{B.21}$$

Now to expand the left-hand side, from vector ψ to the four distinct plant water potential nodes, noting that many derivatives are zero (e.g. $\frac{\delta E_{sun}}{\delta \psi_{sha}} = 0$)

Introducing the notation: $A\Delta\psi = b$

$$\Delta\psi = \begin{bmatrix} \Delta\psi_{sunleaf} \\ \Delta\psi_{shadeleaf} \\ \Delta\psi_{stem} \\ \Delta\psi_{root} \end{bmatrix} \tag{B.22}$$

$$A = \begin{bmatrix} \frac{\delta q_{1a}}{\delta \psi_{sun}} - \frac{\delta E_{sun}}{\delta \psi_{sun}} & 0 & \frac{\delta q_{1a}}{\delta \psi_{stem}} & 0 \\ 0 & \frac{\delta q_{1b}}{\delta \psi_{sha}} - \frac{\delta E_{sha}}{\delta \psi_{sha}} & \frac{\delta q_{1b}}{\delta \psi_{stem}} & 0 \\ -\frac{\delta q_{1a}}{\delta \psi_{sun}} & -\frac{\delta q_{1b}}{\delta \psi_{sha}} & \frac{\delta q_{2}}{\delta \psi_{stem}} - \frac{\delta q_{1a}}{\delta \psi_{stem}} - \frac{\delta q_{1b}}{\delta \psi_{stem}} - \frac{\delta q_{2}}{\delta \psi_{stem}} & \frac{\delta q_{2}}{\delta \psi_{root}} \\ 0 & 0 & \frac{\delta q_{soil}}{\delta \psi_{root}} - \frac{\delta q_{2}}{\delta \psi_{root}} & \end{bmatrix} \tag{B.23}$$

$$b = \begin{bmatrix} E^m_{sun} - q^m_{b1} \\ E^m_{sha} - q^m_{b2} \\ q^m_{b1} + q^m_{b2} - q^m_{stem} \\ q^m_{stem} - q^m_{soil} \end{bmatrix} \tag{B.24}$$

Now we compute all the entries for A and b based on the soil moisture and maximum transpiration forcings and can solve to find:

$$\Delta\psi = A^{-1}b \tag{B.25}$$

$$\psi_{m+1} = \psi_m + \Delta\psi \tag{B.26}$$

We iterate until $b \to 0$, signifying water flux balance through the system. The result is a final set of water potentials ($\psi_{root}, \psi_{xylem}, \psi_{shadeleaf}, \psi_{sunleaf}$) satisfying non-divergent water flux through the system. The magnitude of the water flux is driven by soil matric potential and unstressed ($\beta_t = 1$) transpiration.

We use the transpiration solution (corresponding to the final solution for ψ) to compute stomatal conductance. The stomatal conductance is then used to compute β_t.

$$\beta_{t,sun} = \frac{g_{s,sun}}{g_{s,sun,\beta_t=1}} \tag{B.27}$$

$$\beta_{t,shade} = \frac{g_{s,shade}}{g_{s,shade,\beta_t=1}} \tag{B.28}$$

The β_t values are used in the Photosynthesis module (see section 2.1) to apply water stress. The solution for ψ is saved as a new variable (vegetation water potential) and is indicative of plant water status. The soil-to-root fluxes $(q_{3,1}, q_{3,2}, ..., q_{3,n})$ are used as the soil transpiration sink in the Richards' equation subsurface flow equations.

Furthermore several simplifications were made that decrease the numerical complexity. For the purposes of the PHS solution, soil potentials are assumed constant during each timestep. Plant tissue water storage (capacitance) is not represented, whereby the solution does not depend on the previous timestep and has no time derivatives.

Acknowledgments

= enter acknowledgments here =

PIerre: Text I removed While there are disagreements about soil moisture trends globally [*Dai*, 2013; *Sheffield et al.*, 2012], Amazonia has experienced and a lengthening dry season [*Fu et al.*, 2013] and faces projections of increasing frequency of extreme El Niño events [*Cai et al.*, 2014]

References

Allen, C. D., A. K. Macalady, H. Chenchouni, D. Bachelet, N. McDowell, M. Vennetier, T. Kitzberger, A. Rigling, D. D. Breshears, E. T. Hogg, P. Gonzalez, R. Fensham, Z. Zhang, J. Castro, N. Demidova, J.-H. Lim, G. Allard, S. W. Running, A. Semerci, and N. Cobb (2010), A global overview of drought and heat-induced tree mortality reveals emerging climate change risks for forests, *Forest Ecology and Management*, *259*(4), 660 – 684, doi:https://doi.org/10.1016/j.foreco.2009.09.001.

Anderegg, W. R. L. (2015a), Spatial and temporal variation in plant hydraulic traits and their relevance for climate change impacts on vegetation, *New Phytologist*, *205*(3), 1008–1014, doi:10.1111/nph.12907.

Anderegg, W. R. L., J. M. Kane, and L. D. L. Anderegg (2013a), Consequences of widespread tree mortality triggered by drought and temperature stress, *Nature Climate Change*, *3*(1), 30–36.

Anderegg, W. R. L., L. Plavcová, L. D. L. Anderegg, U. G. Hacke, J. A. Berry, and C. B. Field (2013b), Drought's legacy: multiyear hydraulic deterioration underlies widespread aspen forest die-off and portends increased future risk, *Global Change Biology*, *19*(4), 1188–1196, doi:10.1111/gcb.12100.

Anderegg, W. R. L., C. Schwalm, F. Biondi, J. J. Camarero, G. Koch, M. Litvak, K. Ogle, J. D. Shaw, E. Shevliakova, A. P. Williams, A. Wolf, E. Ziaco, and S. Pacala (2015b), Pervasive drought legacies in forest ecosystems and their implications for carbon cycle models, *Science*, *349*(6247), 528–532, doi:10.1126/science.aab1833.

Bartlett, M. K., T. Klein, S. Jansen, B. Choat, and L. Sack (2016), The correlations and sequence of plant stomatal, hydraulic, and wilting responses to drought, *Proceedings of the National Academy of Sciences*, *113*(46), 13,098–13,103, doi:10.1073/pnas.1604088113.

Bonan, G. B., P. J. Lawrence, K. W. Oleson, S. Levis, M. Jung, M. Reichstein, D. M. Lawrence, and S. C. Swenson (2011), Improving canopy processes in the Community Land Model version 4 (CLM4) using global flux fields empirically inferred from FLUXNET data, *Journal of Geophysical Research*, *116*, doi:10.1029/2010JG001593.

Bonan, G. B., M. Williams, R. A. Fisher, and K. W. Oleson (2014), Modeling stomatal conductance in the earth system: linking leaf water-use efficiency and water transport along the soil-plant-atmosphere continuum, *Geoscientific Model Development*, *7*(5), 2193–2222, doi:10.5194/gmd-7-2193-2014.

Brooks, J. R., F. C. Meinzer, J. M. Warren, J.-C. Domec, and R. Coulombe (2006), Hydraulic redistribution in a douglas-fir forest: lessons from system manipulations, *Plant, Cell & Environment*, *29*(1), 138–150, doi:10.1111/j.1365-3040.2005.01409.x.

Burgess, S. S. O., M. A. Adams, N. C. Turner, and C. K. Ong (1998), The redistribution of soil water by tree root systems, *Oecologia*, *115*(3), 306–311, doi:10.1007/s004420050521.

Cai, W., S. Borlace, M. Lengaigne, P. Van Rensch, M. Collins, G. Vecchi, A. Timmermann, A. Santoso, M. J. Mcphaden, L. Wu, M. H. England, G. Wang, E. Guilyardi, and F.-f. Jin (2014), Increasing frequency of extreme El Niño events due to greenhouse warming, *Nature Climate Change*, *4*(2), 111–116.

Celia, M. A., E. T. Bouloutas, and R. L. Zarba (1990), A general mass-conservative numerical solution for the unsaturated flow equation, *Water Resources Research*, *26*(7), 1483–1496, doi:10.1029/WR026i007p01483.

Choat, B., S. Jansen, T. J. Brodribb, H. Cochard, S. Delzon, R. Bhaskar, S. J. Bucci, T. S. Feild, S. M. Gleason, U. G. Hacke, A. L. Jacobsen, F. Lens, H. Maherali, J. MartÃŋnez-Vilalta, S. Mayr, M. Mencuccini, P. J. Mitchell, A. Nardini, J. Pittermann, R. B. Pratt, J. S. Sperry, M. Westoby, I. J. Wright, and A. E. Zanne (2012), Global convergence in the vulnerability of forests to drought, *Nature*, *491*(7426), 752–5.

Christoffersen, B. O., M. Gloor, S. Fauset, N. M. Fyllas, D. R. Galbraith, T. R. Baker, B. Kruijt, L. Rowland, R. A. Fisher, O. J. Binks, S. Sevanto, C. Xu, S. Jansen, B. Choat, M. Mencuccini, N. G. McDowell, and P. Meir (2016), Linking hydraulic traits to tropical forest function in a size-structured and trait-driven model (tfs v.1-hydro), *Geoscientific Model Development*, *9*(11), 4227–4255, doi:10.5194/gmd-9-4227-2016.

Clapp, R. B., and G. M. Hornberger (1978), Empirical equations for some soil hydraulic properties, *Water Resources Research*, *14*(4), 601–604, doi:10.1029/WR014i004p00601.

Collatz, G., J. Ball, C. Grivet, and J. A. Berry (1991), Physiological and environmental regulation of stomatal conductance, photosynthesis and transpiration: a model that includes a laminar boundary layer, *Agricultural and Forest Meteorology*, *54*(2), 107 – 136, doi:http://dx.doi.org/10.1016/0168-1923(91)90002-8.

da Costa, A. C., D. B. Metcalfe, C. E. Doughty, A. A. de Oliveira, G. F. Neto, M. C. da Costa, J. de Athaydes Silva Junior, L. E. Aragão, S. Almeida, D. R. Galbraith, L. M. Rowland, P. Meir, and Y. Malhi (2014), Ecosystem respiration and net primary productivity after 8-10 years of experimental through-fall reduction in an eastern Amazon forest, *Plant Ecology & Diversity*, *7*(1-2), 7–24, doi:10.1080/17550874.2013.798366.

da Costa, A. C. L., D. Galbraith, S. Almeida, B. Takeshi, T. Portela, M. da Costa, J. ao de Athaydes Silva Junior, A. P. Braga, P. H. L. de Gonçalves, A. A. de Oliveira, R. Fisher, O. L. Phillips, D. B. Metcalfe, P. Levy, and P. Meir (2010), Effect of 7 yr of experimental drought on vegetation dynamics and biomass storage of an eastern amazonian rainforest, *The New Phytologist*, *187*(3), 579–591.

Dai, A. (2013), Increasing drought under global warming in observations and models, *Nature Climate Change*, *3*(1), 52–58.

Dai, Y., R. E. Dickinson, and Y.-P. Wang (2004), A two-big-leaf model for canopy temperature, photosynthesis, and stomatal conductance, *Journal of Climate*, *17*(12), 2281–2299, doi:10.1175/1520-0442(2004)017<2281:ATMFCT>2.0.CO;2.

De Kauwe, M. G., J. Kala, Y.-S. Lin, A. J. Pitman, B. E. Medlyn, R. A. Duursma, G. Abramowitz, Y.-P. Wang, and D. G. Miralles (2015), A test of an optimal stomatal conductance scheme within the CABLE land surface model, *Geoscientific Model Development*, *8*(2), 431–452, doi:10.5194/gmd-8-431-2015.

De Kauwe, M. G., B. E. Medlyn, J. Knauer, and C. A. Williams (2017), Ideas and perspectives: how coupled is the vegetation to the boundary layer?, *Biogeosciences*, *14*(19), 4435–4453, doi:10.5194/bg-14-4435-2017.

Domec, J.-C., J. S. King, A. Noormets, E. Treasure, M. J. Gavazzi, G. Sun, and S. G. McNulty (2010), Hydraulic redistribution of soil water by roots affects whole-stand evapotranspiration and net ecosystem carbon exchange, *The New Phytologist*, *187*(1), 171–183, doi:10.1111/j.1469-8137.2010.03245.x.

Drake, J., S. Power, R. Duursma, B. Medlyn, M. Aspinwall, B. Choat, D. Creek, D. Eamus, C. Maier, S. Pfautsch, R. Smith, M. Tjoelker, and D. Tissue (2017), Stomatal and non-stomatal limitations of photosynthesis for four tree species under drought: A comparison of model formulations, *Agricultural and Forest Meteorology*, *247*, 454 – 466, doi:https://doi.org/10.1016/j.agrformet.2017.08.026.

Egea, G., A. Verhoef, and P. L. Vidale (2011), Towards an improved and more flexible representation of water stress in coupled photosynthesis-stomatal conductance models, *Agricultural and Forest Meteorology*, *151*(10), 1370 – 1384, doi:https://doi.org/10.1016/j.agrformet.2011.05.019.

Entekhabi, D., E. G. Njoku, P. E. O'Neill, K. H. Kellogg, W. T. Crow, W. N. Edelstein, J. K. Entin, S. D. Goodman, T. J. Jackson, J. Johnson, J. Kimball, J. R. Piepmeier, R. D. Koster, N. Martin, K. C. McDonald, M. Moghaddam, S. Moran, R. Reichle, J. C. Shi, M. W. Spencer, S. W. Thurman, L. Tsang, and J. V. Zyl (2010), The soil moisture active passive (smap) mission, *Proceedings of the IEEE*, *98*(5), 704–716, doi:10.1109/JPROC.2010.2043918.

Epila, J., N. J. De Baerdemaeker, L. L. Vergeynst, W. H. Maes, H. Beeckman, and K. Steppe (2017), Capacitive water release and internal leaf water relocation delay drought-induced cavitation in African Maesopsis eminii, *Tree Physiology*, *37*(4), 481–490, doi:10.1093/treephys/tpw128.

Farquhar, G. D., S. von Caemmerer, and J. A. Berry (1980), A biochemical model of photosynthetic CO_2 assimilation in leaves of C_3 species, *Planta*, *149*(1), 78–90, doi:10.1007/BF00386231.

Ficklin, D. L., and K. A. Novick (2017), Historic and projected changes in vapor pressure deficit suggest a continentalâĂŘscale drying of the United States atmosphere, *Journal of Geophysical Research: Atmospheres*, *122*(4), 2061–2079, doi:10.1002/2016JD025855.

Fisher, R. A., M. Williams, R. L. Do Vale, A. L. Da Costa, and P. Meir (2006), Evidence from Amazonian forests is consistent with isohydric control of leaf water potential, *Plant, Cell & Environment*, *29*(2), 151–165, doi:10.1111/j.1365-3040.2005.01407.x.

Fisher, R. A., M. Williams, A. L. D. Costa, Y. Malhi, R. F. D. Costa, S. Almeida, and P. Meir (2007), The response of an Eastern Amazonian rain forest to drought stress: results and modelling analyses from a throughfall exclusion experiment, *Global Change Biology*, *13*(11), 2361–2378, doi:10.1111/j.1365-2486.2007.01417.x.

Fisher, R. A., M. Williams, M. de Lourdes Ruivo, A. L. de Costa, and P. Meir (2008), Evaluating climatic and soil water controls on evapotranspiration at two Amazonian rainforest sites, *Agricultural and Forest Meteorology*, *148*(6), 850 – 861, doi: https://doi.org/10.1016/j.agrformet.2007.12.001.

Flexas, J., J. Bota, F. Loreto, G. Cornic, and T. D. Sharkey (2004), Diffusive and metabolic limitations to photosynthesis under drought and salinity in c3 plants, *Plant Biology*, *6*(3), 269–279, doi:10.1055/s-2004-820867.

Flexas, J., M. Ribas-Carbó, J. Bota, J. Galmés, M. Henkle, S. Martínez-Cañellas, and H. Medrano (2006), Decreased rubisco activity during water stress is not induced by decreased relative water content but related to conditions of low stomatal conductance and chloroplast CO2 concentration, *New Phytologist*, *172*(1), 73–82, doi:10.1111/j.1469-8137.2006.01794.x.

Franks, P. J., P. L. Drake, and R. H. Froend (2007), Anisohydric but isohydrodynamic: seasonally constant plant water potential gradient explained by a stomatal control mechanism incorporating variable plant hydraulic conductance, *Plant, Cell & Environment*, *30*(1), 19–30, doi:10.1111/j.1365-3040.2006.01600.x.

Friedlingstein, P., M. Meinshausen, V. K. Arora, C. D. Jones, A. Anav, S. K. Liddicoat, and R. Knutti (2014), Uncertainties in CMIP5 climate projections due to carbon cycle feedbacks, *Journal of Climate*, *27*(2), 511–526.

Fu, R., L. Yin, W. Li, P. A. Arias, R. E. Dickinson, L. Huang, S. Chakraborty, K. Fernandes, B. Liebmann, R. Fisher, and R. B. Myneni (2013), Increased dry-season length over southern Amazonia in recent decades and its implication for future climate projection, *Proceedings of the National Academy of Sciences of the United States of America*, *110*(45), 18,110–18,115.

Gentine, P., M. Guérin, M. Uriarte, N. G. McDowell, and W. T. Pockman (2016), An allometry-based model of the survival strategies of hydraulic failure and carbon starvation, *Ecohydrology*, *9*(3), 529–546, doi:10.1002/eco.1654.

Grant, J., J.-P. Wigneron, R. D. Jeu, H. Lawrence, A. Mialon, P. Richaume, A. A. Bitar, M. Drusch, M. van Marle, and Y. Kerr (2016), Comparison of SMOS and AMSR-E vegetation optical depth to four MODIS-based vegetation indices, *Remote Sensing of Environment*, *172*, 87 – 100, doi:https://doi.org/10.1016/j.rse.2015.10.021.

Green, J. K., A. G. Konings, S. H. Alemohammad, J. Berry, D. Entekhabi, J. Kolassa, J.-E. Lee, and P. Gentine (2017), Regionally strong feedbacks between the atmosphere and terrestrial biosphere, *Nature Geoscience*, *10*(6), 410–414, doi:10.1038/ngeo2957.

Harley, P. C., R. B. Thomas, J. F. Reynolds, and B. R. Strain (1992), Modelling photosynthesis of cotton grown in elevated co2, *Plant Cell Environment*, *15*(3), 271–282, doi: 10.1111/j.1365-3040.1992.tb00974.x.

Holbrook, N. M., E. T. Ahrens, M. J. Burns, and M. A. Zwieniecki (2001), In vivo observation of cavitation and embolism repair using magnetic resonance imaging, *Plant Physiology*, *126*(1), 27–31, doi:10.1104/pp.126.1.27.

Jackson, R. B., J. Canadell, J. R. Ehleringer, H. A. Mooney, O. E. Sala, and E. D. Schulze (1996), A global analysis of root distributions for terrestrial biomes, *Oecologia*, *108*(3), 389–411, doi:10.1007/BF00333714.

Joetzjer, E., C. Delire, H. Douville, P. Ciais, B. Decharme, R. Fisher, B. Christoffersen, J. C. Calvet, A. C. L. da Costa, L. V. Ferreira, and P. Meir (2014), Predicting the response of the Amazon rainforest to persistent drought conditions under current and future climates: a major challenge for global land surface models, *Geoscientific Model Development*, *7*(6), 2933–2950, doi:10.5194/gmd-7-2933-2014.

Kattge, J., S. DÃŊAz, S. Lavorel, I. C. Prentice, P. Leadley, G. BÃŰNisch, E. Garnier, M. Westoby, P. B. Reich, I. J. Wright, J. H. C. Cornelissen, C. Violle, S. P. Harri-

son, P. M. Van Bodegom, M. ReichSTEIN, B. J. Enquist, N. A. Soudzilovskaia, D. D. Ackerly, M. Anand, O. Atkin, M. Bahn, T. R. Baker, D. Baldocchi, R. Bekker, C. C. Blanco, B. Blonder, W. J. Bond, R. Bradstock, D. E. Bunker, F. Casanoves, J. Cavender-Bares, J. Q. Chambers, F. S. Chapin Iii, J. Chave, D. Coomes, W. K. Cornwell, J. M. Craine, B. H. Dobrin, L. Duarte, W. Durka, J. Elser, G. Esser, M. Estiarte, W. F. Fagan, J. Fang, F. FernÃĄNdez-MÃĽNdez, A. Fidelis, B. Finegan, O. Flores, H. Ford, D. Frank, G. T. Freschet, N. M. Fyllas, R. V. Gallagher, W. A. Green, A. G. Gutierrez, T. Hickler, S. I. Higgins, J. G. Hodgson, A. Jalili, S. Jansen, C. A. Joly, A. J. Kerkhoff, D. Kirkup, K. Kitajima, M. Kleyer, S. Klotz, J. M. H. Knops, K. Kramer, I. KÃIJHn, H. Kurokawa, D. Laughlin, T. D. Lee, M. Leishman, F. Lens, T. Lenz, S. L. Lewis, J. Lloyd, J. LlusiÃĂ, F. Louault, S. Ma, M. D. MaHECHA, P. MaNNING, T. MaSSAD, B. E. Medlyn, J. Messier, A. T. Moles, S. C. MÃIJLler, K. Nadrowski, S. Naeem, Ã. Niinemets, S. NÃŰLlerT, A. NÃIJSke, R. Ogaya, J. Oleksyn, V. G. Onipchenko, Y. Onoda, J. OrdoÃŚEz, G. Overbeck, W. A. Ozinga, S. PatiÃŚO, S. Paula, J. G. Pausas, J. PeÃŚUelas, O. L. Phillips, V. Pillar, H. Poorter, L. Poorter, P. Poschlod, A. Prinzing, R. Proulx, A. Rammig, S. Reinsch, B. Reu, L. Sack, B. Salgado-Negret, J. Sardans, S. Shiodera, B. Shipley, A. Siefert, E. Sosinski, J.-F. Soussana, E. Swaine, N. Swenson, K. Thompson, P. Thornton, M. Waldram, E. Weiher, M. White, S. White, S. J. Wright, B. Yguel, S. Zaehle, A. E. Zanne, and C. Wirth (2011), Try âĂŞ a global database of plant traits, *Global Change Biology*, *17*(9), 2905–2935, doi:10.1111/j.1365-2486.2011.02451.x.

Klein, T., and S. Niu (2014), The variability of stomatal sensitivity to leaf water potential across tree species indicates a continuum between isohydric and anisohydric behaviours, *Functional Ecology*, *28*(6), 1313–1320, doi:10.1111/1365-2435.12289.

Konings, A. G., and P. Gentine (2017a), Global variations in ecosystem-scale isohydricity, *Global Change Biology*, *23*(2), 891–905, doi:10.1111/gcb.13389.

Konings, A. G., M. Piles, K. RÃűtzer, K. A. McColl, S. K. Chan, and D. Entekhabi (2016), Vegetation optical depth and scattering albedo retrieval using time series of dual-polarized l-band radiometer observations, *Remote Sensing of Environment*, *172*, 178 – 189, doi:https://doi.org/10.1016/j.rse.2015.11.009.

Konings, A. G., A. P. Williams, and P. Gentine (2017b), Sensitivity of grassland productivity to aridity controlled by stomatal and xylem regulation, *Nature Geoscience*, *10*(4), 284–288, doi:10.1038/ngeo2903.

Lee, J.-E., R. S. Oliveira, T. E. Dawson, and I. Fung (2005), Root functioning modifies seasonal climate, *Proceedings of the National Academy of Sciences of the United States of America*, *102*(49), 17,576–17,581, doi:10.1073/pnas.0508785102.

Lin, C., P. Gentine, Y. Huang, K. Guan, H. Kimm, and S. Zhou (2018), Diel ecosystem conductance response to vapor pressure deficit is suboptimal and independent of soil moisture, *Agricultural and Forest Meteorology*, *250-251*, 24 – 34, doi:https://doi.org/10.1016/j.agrformet.2017.12.078.

Mackay, D. S., D. E. Roberts, B. E. Ewers, J. S. Sperry, N. G. McDowell, and W. T. Pockman (2015), Interdependence of chronic hydraulic dysfunction and canopy processes can improve integrated models of tree response to drought, *Water Resources Research*, *51*(8), 6156–6176, doi:10.1002/2015WR017244.

Manzoni, S., G. Vico, G. Katul, P. A. Fay, W. Polley, S. Palmroth, and A. Porporato (2011), Optimizing stomatal conductance for maximum carbon gain under water stress: a meta-analysis across plant functional types and climates, *Functional Ecology*, *25*(3), 456–467, doi:10.1111/j.1365-2435.2010.01822.x.

Manzoni, S., G. Vico, S. Palmroth, A. Porporato, and G. Katul (2013a), Optimization of stomatal conductance for maximum carbon gain under dynamic soil moisture, *Advances in Water Resources*, *62*, 90 – 105, doi:https://doi.org/10.1016/j.advwatres.2013.09.020.

Manzoni, S., G. Vico, G. Katul, S. Palmroth, R. B. Jackson, and A. Porporato (2013b), Hydraulic limits on maximum plant transpiration and the emergence of the safety-efficiency trade-off, *New Phytologist*, *198*(1), 169–178, doi:10.1111/nph.12126.

Mcdowell, N. G., and C. D. Allen (2015), Darcy's law predicts widespread forest mortality under climate warming, *Nature Climate Change*, *5*(7), 669–672.

McDowell, N. G., R. A. Fisher, C. Xu, J. C. Domec, T. HÃűlttÃď, D. S. Mackay, J. S. Sperry, A. Boutz, L. Dickman, N. Gehres, J. M. Limousin, A. Macalady, J. MartÃŋnez-Vilalta, M. Mencuccini, J. A. Plaut, J. OgÃľe, R. E. Pangle, D. P. Rasse, M. G. Ryan, S. Sevanto, R. H. Waring, A. P. Williams, E. A. Yepez, and W. T. Pockman (2013), Evaluating theories of drought-induced vegetation mortality using a multimodelâĂŞexperiment framework, *New Phytologist*, *200*(2), 304–321, doi:10.1111/nph.12465.

McDowell, N. G., A. P. Williams, C. Xu, W. T. Pockman, L. T. Dickman, S. Sevanto, R. Pangle, J. Limousin, J. Plaut, D. S. Mackay, J. Ogee, J. C. Domec, C. D. Allen, R. A. Fisher, X. Jiang, J. D. Muss, D. D. Breshears, S. A. Rauscher, and C. Koven (2016), Multi-scale predictions of massive conifer mortality due to chronic temperature rise, *Nature Climate Change*, *6*, 295–300, doi:10.1038/nclimate2873.

Medlyn, B. E., R. A. Duursma, D. Eamus, D. S. Ellsworth, I. C. Prentice, C. V. M. Barton, K. Y. Crous, P. De Angelis, M. Freeman, and L. Wingate (2011), Reconciling the optimal and empirical approaches to modelling stomatal conductance, *Global Change Biology*, *17*(6), 2134–2144, doi:10.1111/j.1365-2486.2010.02375.x.

Meinzer, F. C., S. A. James, and G. Goldstein (2004), Dynamics of transpiration, sap flow and use of stored water in tropical forest canopy trees, *Tree Physiology*, *24*(8), 901–909, doi:10.1093/treephys/24.8.901.

Meinzer, F. C., D. M. Johnson, B. Lachenbruch, K. A. McCulloh, and D. R. Woodruff (2009), Xylem hydraulic safety margins in woody plants: coordination of stomatal control of xylem tension with hydraulic capacitance, *Functional Ecology*, *23*(5), 922–930, doi:10.1111/j.1365-2435.2009.01577.x.

Momen, M., J. D. Wood, K. A. Novick, R. Pangle, W. T. Pockman, N. G. McDowell, and A. G. Konings (2017), Interacting effects of leaf water potential and biomass on vegetation optical depth, *Journal of Geophysical Research: Biogeosciences*, *122*(11), 3031–3046, doi:10.1002/2017JG004145.

Nepstad, D. C., R. de Carvalho, Claudio, E. A. Davidson, P. H. Jipp, and e. al (1994), The role of deep roots in the hydrological and carbon cycles of amazonian forests and pastures, *Nature*, *372*(6507), 666.

Novick, K. A., D. L. Ficklin, P. C. Stoy, C. A. Williams, G. Bohrer, A. Oishi, S. A. Papuga, P. D. Blanken, A. Noormets, B. N. Sulman, R. L. Scott, L. Wang, and R. P. Phillips (2016a), The increasing importance of atmospheric demand for ecosystem water and carbon fluxes, *Nature Climate Change*, *6*(11), 1023–1027.

Novick, K. A., C. F. Miniat, and J. M. Vose (2016b), Drought limitations to leaf-level gas exchange: results from a model linking stomatal optimization and cohesion-tension theory, *Plant, Cell & Environment*, *39*(3), 583–596, doi:10.1111/pce.12657.

Oleson, K. W., D. M. Lawrence, G. B. Bonan, B. Drewniak, M. Huang, C. D. Koven, S. Levis, F. Li, W. J. Riley, Z. M. Subin, S. C. Swenson, P. E. Thornton, A. Bozbiyik, R. Fisher, C. L. Heald, E. Kluzek, J.-F. Lamarque, P. J. Lawrence, L. R. Leung, W. Lipscomb, S. Muszala, D. M. Ricciuto, W. Sacks, Y. Sun, J. Tang, and Z.-L. Yang (2013), Technical description of version 4.5 of the community land model (clm), NCAR Tech. Note NCAR/TN-503+STR, *National Center for Atmospheric Research, Boulder, Colorado, 420 pp.*, doi:10.5065/D6RR1W7M.

Oliveira, R. S., T. E. Dawson, S. S. O. Burgess, and D. C. Nepstad (2005), Hydraulic redistribution in three amazonian trees, *Oecologia*, *145*(3), 354–363, doi:10.1007/s00442-005-0108-2.

Powell, T. L., D. R. Galbraith, B. O. Christoffersen, A. Harper, H. M. A. Imbuzeiro, L. Rowland, S. Almeida, P. M. Brando, A. C. L. da Costa, M. H. Costa, N. M. Levine, Y. Malhi, S. R. Saleska, E. Sotta, M. Williams, P. Meir, and P. R. Moorcroft (2013), Confronting model predictions of carbon fluxes with measurements of amazon forests subjected to experimental drought, *New Phytologist*, *200*(2), 350–365, doi:10.1111/nph.12390.

Restaino, C. M., D. L. Peterson, and J. Littell (2016), Increased water deficit decreases douglas fir growth throughout western US forests, *Proceedings of the National Academy of Sciences*, *113*(34), 9557–9562, doi:10.1073/pnas.1602384113.

Restrepo-Coupe, N., N. M. Levine, B. O. Christoffersen, L. P. Albert, J. Wu, M. H. Costa, D. Galbraith, H. Imbuzeiro, G. Martins, A. C. da Araujo, Y. S. Malhi, X. Zeng, P. Moorcroft, and S. R. Saleska (2017), Do dynamic global vegetation models capture the seasonality of carbon fluxes in the amazon basin? A data-model intercomparison, *Global Change Biology*, *23*(1), 191–208, doi:10.1111/gcb.13442.

Sack, L., P. J. Melcher, M. A. Zwieniecki, and N. M. Holbrook (2002), The hydraulic conductance of the angiosperm leaf lamina: a comparison of three measurement methods, *Journal of Experimental Botany*, *53*(378), 2177–2184.

Scholz, F. G., N. G. Phillips, S. J. Bucci, F. C. Meinzer, and G. Goldstein (2011), Hydraulic capacitance: Biophysics and functional significance of internal water sources, in Meinzer, F.C., Lachenbruch, B., Dawson, T. E. (eds) *Size- and Age-Related Changes in Tree Structure and Function*, pp. 341–361, Springer, Dordrecht.

Seager, R., A. Hooks, A. P. Williams, B. Cook, J. Nakamura, and N. Henderson (2015), Climatology, variability, and trends in the u.s. vapor pressure deficit, an important fire-related meteorological quantity, *Journal of Applied Meteorology and Climatology*, *54*(6), 1121–1141, doi:10.1175/JAMC-D-14-0321.1.

Sellers, P. J., D. A. Randall, G. J. Collatz, J. A. Berry, C. B. Field, D. A. Dazlich, C. Zhang, G. D. Collelo, and L. Bounoua (1996a), a revised land surface parameterization (sib2) for atmospheric gcms. part i: Model formulation, *Journal of Climate*, *9*(4), 676–705, doi:10.1175/1520-0442(1996)009<0676:ARLSPF>2.0.CO;2.

Sellers, P. J., C. J. Tucker, G. J. Collatz, S. O. Los, C. O. Justice, D. A. Dazlich, and D. A. Randall (1996b), A revised land surface parameterization (sib2) for atmospheric gcms. part ii: The generation of global fields of terrestrial biophysical parameters from satellite data, *Journal of Climate*, *9*(4), 706–737, doi:10.1175/1520-0442(1996)009<0706:ARLSPF>2.0.CO;2.

Sheffield, J., E. F. Wood, and M. L. Roderick (2012), Little change in global drought over the past 60 years, *Nature*, *491*(7424), 435–8.

Simonin, K. A., E. Burns, B. Choat, M. M. Barbour, T. E. Dawson, and P. J. Franks (2015), Increasing leaf hydraulic conductance with transpiration rate minimizes the water potential drawdown from stem to leaf, *Journal of Experimental Botany*, *66*(5), 1303–1315, doi:10.1093/jxb/eru481.

Siqueira, M., G. Katul, and A. Porporato (2008), Onset of water stress, hysteresis in plant conductance, and hydraulic lift: Scaling soil water dynamics from millimeters to meters, *Water Resources Research*, *44*(1), W01,432, doi:10.1029/2007WR006094.

Sperry, J. S., and D. M. Love (2015), What plant hydraulics can tell us about responses to climate-change droughts, *New Phytologist*, *207*(1), 14–27, doi:10.1111/nph.13354.

Sperry, J. S., F. R. Adler, G. S. Campbell, and J. P. Comstock (1998), Limitation of plant water use by rhizosphere and xylem conductance: results from a model, *Plant Cell Environment*, *21*(4), 347–359, doi:10.1046/j.1365-3040.1998.00287.x.

Sperry, J. S., U. G. Hacke, R. Oren, and J. P. Comstock (2002), Water deficits and hydraulic limits to leaf water supply, *Plant, Cell & Environment*, *25*(2), 251–263, doi:10.1046/j.0016-8025.2001.00799.x.

Sperry, J. S., M. D. Venturas, W. R. L. Anderegg, M. Mencuccini, D. S. Mackay, Y. Wang, and D. M. Love (2017), Predicting stomatal responses to the environment from the optimization of photosynthetic gain and hydraulic cost, *Plant, Cell & Environment*, *40*(6), 816–830, doi:10.1111/pce.12852, pCE-16-0541.R1.

Thornton, P. E., and N. E. Zimmermann (2007), An improved canopy integration scheme for a land surface model with prognostic canopy structure, *Journal of Climate*, *20*(15), 3902–3923, doi:10.1175/JCLI4222.1.

Tyree, M. T., and J. S. Sperry (1988), Do woody plants operate near the point of catastrophic xylem dysfunction caused by dynamic water stress?: Answers from a model, *Plant Physi-*

ology, *88*(3), 574–580.

Tyree, M. T., and J. S. Sperry (1989), Vulnerability of xylem to cavitation and embolism, *Annual Review of Plant Physiology and Plant Molecular Biology*, *40*(1), 19–36, doi: 10.1146/annurev.pp.40.060189.000315.

Ukkola, A. M., M. G. D. Kauwe, A. J. Pitman, M. J. Best, G. Abramowitz, V. Haverd, M. Decker, and N. Haughton (2016), Land surface models systematically overestimate the intensity, duration and magnitude of seasonal-scale evaporative droughts, *Environmental Research Letters*, *11*(10), 104,012.

Verhoef, A., and G. Egea (2014), Modeling plant transpiration under limited soil water: Comparison of different plant and soil hydraulic parameterizations and preliminary implications for their use in land surface models, *Agricultural and Forest Meteorology*, *191*, 22–32, doi:https://doi.org/10.1016/j.agrformet.2014.02.009.

Williams, A. P., C. D. Allen, A. K. Macalady, D. Griffin, C. A. Woodhouse, D. M. Meko, T. W. Swetnam, S. A. Rauscher, R. Seager, H. Grissino-Mayer, J. S. Dean, E. R. Cook, C. Gangodagamage, M. Cai, and N. G. Mcdowell (2013), Temperature as a potent driver of regional forest drought stress and tree mortality, *Nature Climate Change*, *3*(3), 292–297.

Williams, M., E. B. Rastetter, D. N. Fernandes, M. L. Goulden, S. C. Wofsy, G. R. Shaver, J. M. Melillo, J. W. Munger, S.-M. Fan, and K. J. Nadelhoffer (1996), Modelling the soil-plant-atmosphere continuum in a quercusâĂŞacer stand at harvard forest: the regulation of stomatal conductance by light, nitrogen and soil/plant hydraulic properties, *Plant, Cell & Environment*, *19*(8), 911–927, doi:10.1111/j.1365-3040.1996.tb00456.x.

Williams, M., B. E. Law, P. M. Anthoni, and M. H. Unsworth (2001), Use of a simulation model and ecosystem flux data to examine carbonâĂŞwater interactions in ponderosa pine., *Tree Physiology*, *21*(5), 287 – 298.

Xu, X., D. Medvigy, J. S. Powers, J. M. Becknell, and K. Guan (2016), Diversity in plant hydraulic traits explains seasonal and inter-annual variations of vegetation dynamics in seasonally dry tropical forests, *New Phytologist*, *212*(1), 80–95, doi:10.1111/nph.14009, 2015-20772.

Zhou, S., R. A. Duursma, B. E. Medlyn, J. W. Kelly, and I. C. Prentice (2013), How should we model plant responses to drought? An analysis of stomatal and non-stomatal responses to water stress, *Agricultural and Forest Meteorology*, *182-183*, 204 – 214, doi: https://doi.org/10.1016/j.agrformet.2013.05.009.

Zhou, S., B. Medlyn, S. Sabaté, D. Sperlich, I. C. Prentice, and D. Whitehead (2014), Short-term water stress impacts on stomatal, mesophyll and biochemical limitations to photosynthesis differ consistently among tree species from contrasting climates, *Tree Physiology*, *34*(10), 1035, doi:10.1093/treephys/tpu072.